

RESEARCH ARTICLE | MAY 08 2025

Transition path dynamics for one-dimensional run and tumble particle

Special Collection: [Anomalous Diffusion and Fluctuations in Complex Systems and Networks](#)

Hua Li ; Yong Xu  ; Ralf Metzler ; Jianwei Shen ; Kheder Suleiman 

 Check for updates

Chaos 35, 053132 (2025)

<https://doi.org/10.1063/5.0249277>



Articles You May Be Interested In

Bio-inspired *in silico* microswimmer: Run and tumble kinematics

Physics of Fluids (March 2023)

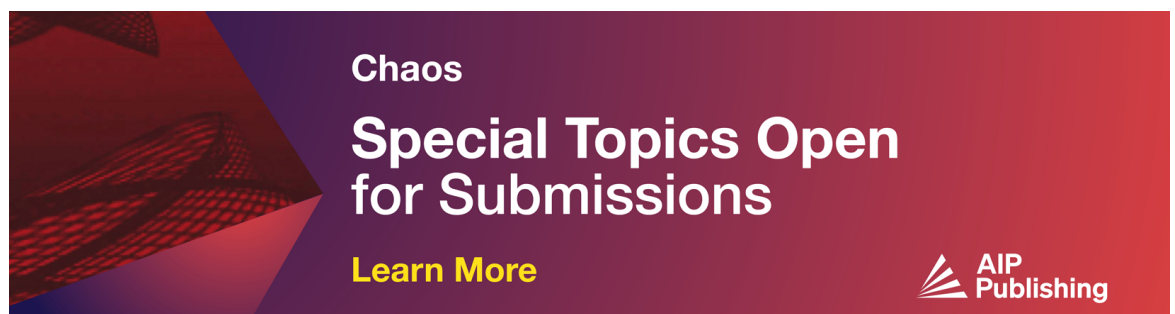
Run-and-tumble particles in slit geometry as a splitting probability problem

Physics of Fluids (November 2024)


Inertial dynamics of run-and-tumble particle

Chaos (March 2025)

09 May 2025 05:44:22



Chaos
**Special Topics Open
for Submissions**
[Learn More](#)



Transition path dynamics for one-dimensional run and tumble particle

Cite as: Chaos 35, 053132 (2025); doi: 10.1063/5.0249277
Submitted: 16 November 2024 · Accepted: 22 April 2025 ·
Published Online: 8 May 2025



View Online



Export Citation



CrossMark

Hua Li,¹ Yong Xu,^{2,3,a} Ralf Metzler,^{4,5} Jianwei Shen,¹ and Kheder Suleiman²

AFFILIATIONS

¹School of Mathematics and Statistics, North China University of Water Resources and Electric Power, Zhengzhou 450046, China

²Department of Applied Mathematics, Northwestern Polytechnical University, Xi'an 710072, China

³MOE Key Laboratory for Complexity Science in Aerospace, Northwestern Polytechnical University, Xi'an 710072, China

⁴Institute for Physics & Astronomy, University of Potsdam, 14476 Potsdam-Golm, Germany

⁵Asia Pacific Center for Theoretical Physics, Pohang 37673, Republic of Korea

Note: This paper is part of the Focus Issue on Anomalous Diffusion and Fluctuations in Complex Systems and Networks.

^a**Author to whom correspondence should be addressed:** hsux3@nwpu.edu.cn

ABSTRACT

We study transition path properties such as the transient probability density, transition path time and its distribution, splitting probability, coefficient of variation, and the transition path shape of active run and tumble particles for unconstrained motion. In particular, we provide the theoretical description of the transition path properties using forward and backward master equations. The theoretical results are supported by Monte Carlo simulations. In particular, we prove that the system dynamics do not feature a symmetry breaking in the transition path properties for the case of run and tumble particles considered here. The symmetry of the transition path properties is shown to emerge for variations of the particle tumbling rate, particle speed, and transition path region.

Published under an exclusive license by AIP Publishing. <https://doi.org/10.1063/5.0249277>

Active matter is a popular example of non-equilibrium systems, and there are various novel phenomena that are being explored, including the associated transition path properties. The transition path dynamics has been widely explored in physical, chemical, and biological systems. Here, we use this approach for the investigation of the transition path mechanisms of run and tumble particles based on a newly developed theoretical approach. In particular, we illustrate the rich transition path dynamical behaviors of run and tumble particles. The theoretical and numerical results reveal that the tumble rate and velocity of the particles cannot affect the symmetry breaking phenomenon of the transition path dynamics. We argue that our results provide a paradigm for the study of transition path dynamics in active matter.

I. INTRODUCTION

Active matter forms a class of non-equilibrium systems that can self-propel by consuming energy from their surroundings.¹⁻⁵ From the standpoint of statistical physics, active matter provide an ideal simplified model to explore the fundamental aspects

of nonequilibrium systems.⁶ Examples of active systems range from molecular motors,⁷⁻⁹ over synthetic Janus particles,¹⁰ microorganisms such as bacteria,^{11,12} to birds¹³ and fish schools.¹⁴

Self-propelled particles and their ensembles are model systems of active matter. On a more abstract level, for instance, the movement of swarms of mosquitoes were already discussed by Ross in 1902 in the context of malaria spreading¹⁵ and modeled in terms of a random walk by Pearson in 1905.¹⁶ The motion of an individual neutrophil cell chasing a bacterium in a blood smear filmed by David Rogers in the 1950s has become an iconic movie for active motion of single cells.¹⁷ Systematic studies of bacterial motion by flagellar propulsion were conducted by Berg since the 1970s.¹⁸ Based on physical models, in 1987, Reynolds introduced the “Boids model” to numerically simulate the collective motion of land animals and fish schools.¹⁹ In 1995, Vicsek proposed the Vicsek model,²⁰ in which self-propelled particles move at a constant speed, and the direction of motion is influenced by the surrounding particles. This simple and efficient model can be used to reveal the formation mechanism and dynamical characteristics of group dynamical behavior. Such self-propelled particles can be man-made micron-sized or nanoparticles, or biological matter. In recent years, with the continuous

development of colloid science and technology, the synthesis of controllable self-propelled particles has gradually become a basic research object in the field of active matter. Among these, the size of synthetic active Brownian particles is at the micro- to nanometer level,²¹ and due to their easy manufacture, such active particles have been used in a large number of studies in experiments and theories. In particular, active particles can explain the self-propelled behavior of biological individuals in general.²² In biology, self-propulsion is needed, e.g., to search for nutrients to escape predators.

With the study of bacterial movement patterns, the run and tumble particle (RTP) model was developed, and it is now one of the paradigmatic models of self-propelled particles.²³ RTPs perform persistent Brownian motion. The model remains one of the few accurately solvable models of self-propelled particles and is often used as pioneering research to understand more complex phenomena.²⁴ Especially, the work of Berg on the flagellar propulsion of *Escherichia coli* increased the interest in the RTP model, in biological modeling of bacterial motion.²⁵

A remarkable feature of RTPs and other active particles is that they do not satisfy detailed balance, and even at the single-particle level, they exhibit many interesting dynamical behaviors different from those of Brownian particles. Recently, theoretical and experimental studies on RTPs have provided significant new insights, e.g., in the context of positional distributions,^{26,27} stochastic resetting,^{28,29} anomalous transport properties,³⁰ phase transitions,³¹ first passage properties,^{32,33} field theories, and entropy production.^{34,35} Specifically, RTPs have non-equilibrium (non-Boltzmann) steady state distributions in an external potential.^{36,37} In confined regions, the persistence of RTP motion can lead to the accumulation of particles at the boundaries.^{38–40} The resetting of the position and velocity of RTPs result in non-equilibrium stationary states, e.g., Laplace distributions.⁴¹ The first passage time statistic of RTPs no longer satisfies Arrhenius law.^{42,43} Significant progress has been made in the theoretical calculation of the transient probability density of RTPs in the free-diffusion case.⁴⁴ However, despite its seeming simplicity, the RTP model still lacks a precise analytical description of the kinetic behaviors, in particular, for the transition path dynamics.⁴⁵

Here, we are interested in the transition path dynamics of RTPs. Transition paths^{46,47} contain all the key information and are the most important part of capturing the occurrence of escape dynamics behavior. Transition path dynamics include measures of splitting probability, transition path time and its distribution, transition path shape, etc.⁴⁸ Specifically, the transition path time⁴⁹ is the duration of the transition path over the transition region and portrays the time taken by the particle to successfully undergo the true exit behavior.⁵⁰ In molecular systems, the transition path time may be the transition time through the pore of a cell membrane, ion channel transport, or the translocation time of a polymer through a pore.⁵¹ The coefficient of variation (COV) is applied to describe the relative width of a distribution, and it is used in various fields from engineering to economics. In fact, the COV of a distribution is a more robust statistical measure than the distribution itself. In general, the value of the COV is small for narrower distributions, a heavy-tailed distribution has a COV exceeding one, and the COV of exponential distribution equals one.⁵² Meanwhile, the COV of transition path time distribution reveals the dimensionality of the underlying free energy landscape. A COV exceeding one is also a

characteristic of multidimensional dynamics.⁵³ The transition path shape⁵⁴ is a characteristic of the dynamic distribution of time and position of the transition path within the transition region. It is a more detailed measure of the transition path sequence, reflecting better the specific information of the transition path sequence. The transition path shape is a powerful tool for studying the mechanism of rare events such as chemical reactions and conformational transitions of biological macromolecules, and is important for the characterization of the true exit problem of systems.

Over the recent years, many numerical and theoretical studies on transition path dynamics have emerged. A series of efficient simulation methods have been proposed, such as umbrella sampling,⁵⁵ transition interface sampling,⁵⁶ string method,⁵⁷ milestone, ^{58,59} forward flux sampling,^{60,61} and deep learning.^{62–64} Since the theoretical computation of transition paths involves solving the Fokker–Planck equation with two absorbing boundaries, most of the theoretical studies have focused on one-dimensional systems. Subsequently, theoretical studies to include non-Markov effects^{65,66} and different potential functions,^{67–69} noise,^{70,71} and other aspects, have contributed to the physical picture of transition paths. Interestingly, non-equilibrium systems^{72,73} can break the symmetry of the transition path time, e.g., dynamical systems driven by Lévy noise,⁷⁴ Poisson noise,⁷⁵ telegraph noise,⁷⁶ and other non-equilibrium forces. The study of symmetry breaking phenomena in transition paths is crucial for protein conformational analysis, engineering safety design, and clinical drug development.^{77,78} Gladrow⁷⁶ verified experimentally that telegraphic processes can lead to symmetry breaking in the properties of transition paths. To close the gap, we here study analytically the transition path dynamics of RTPs, for which theoretical analyses are still largely pending. At this point, we note that the RTP dynamics can be mapped on the telegraphic process.⁷⁹

Several factors underscore the importance of the study of transition path dynamics of RTPs. First, active matter is inherently governed by non-equilibrium states with novel macroscopic thermodynamic properties.¹ Particularly, recent studies have shown that familiar equilibrium thermodynamic concepts and relationships are not fully applicable to active matter systems, often leading to counterintuitive phenomena.⁸⁰ Furthermore, the study of cell movement has significant implications, as it can reveal the significance of topological defects in biological development,⁸¹ while the research of the transition path dynamics of active matter is expected to provide the possibility for active drug delivery and precision diagnosis and treatment.⁸² Moreover, the transition path dynamics of RTPs received less interest, and most results relevant to active particles are limited to the case of Gaussian colored noise. The transition path dynamics of RTPs is subject to further study.⁸³ Therefore, the transition path properties of run and tumble particles reflect an important aspect of the complete stochastic theory of RTPs.

The paper is structured as follows. In Sec. II, the theoretical derivation of the transient probability density, transition path time distribution, splitting probability, transition path time, COV and transition path shape of a free RTP are studied in detail starting from the forward and backward master equations. Subsequently, in Sec. III, the numerical simulation method for the system is detailed. Then, the theoretical approach is applied to the transition path region and transition path properties of RTPs in Sec. IV. Finally, the concluding part of the paper is presented. Some specific procedures

for the theoretical calculation of the transition path properties are collected in the Appendices.

II. TRANSITION PATH PROPERTIES OF RUN AND TUMBLE PARTICLES

Consider a free RTP confined to the transition region $[x_A, x_B]$, where x_A and x_B are the locations of two absorbing boundaries. The position $x(t)$ of the particle is modeled in terms of the Langevin equation⁸⁴

$$\frac{dx(t)}{dt} = v\sigma(t), \tag{1}$$

where $x(t)$ is the so-called persistent Brownian walk, in which v is the particle speed. $\sigma(t)$ is a dichotomous noise that assumes the values ± 1 with a Poissonian tumbling rate γ . Here, $\sigma(t) = +1$ and -1 mean that the particle is in the “right-moving” and “left-moving” state, respectively.

The forward master equations corresponding to Eq. (1) read

$$\begin{aligned} \frac{\partial P_+(x, t|x_0, \sigma_j)}{\partial t} &= -v \frac{\partial}{\partial x} P_+(x, t|x_0, \sigma_j) - \gamma [P_+(x, t|x_0, \sigma_j) - P_-(x, t|x_0, \sigma_j)], \end{aligned} \tag{2a}$$

$$\begin{aligned} \frac{\partial P_-(x, t|x_0, \sigma_j)}{\partial t} &= v \frac{\partial}{\partial x} P_-(x, t|x_0, \sigma_j) + \gamma [P_+(x, t|x_0, \sigma_j) - P_-(x, t|x_0, \sigma_j)], \end{aligned} \tag{2b}$$

where $P_+(x, t|x_0, \sigma_j)$ and $P_-(x, t|x_0, \sigma_j)$ denote the probability density functions (PDFs) for the particle to be at position x at time t with velocity $\sigma(t) = \pm 1$, under the condition that the particle was initially located at x_0 with $\sigma_j = \pm 1$, respectively. Equations (2a) and (2b) are coupled differential equations. The initial conditions are explicitly given by

$$P_{\pm}(x, t|x_0, \sigma_j) = \delta_{\sigma_j, \pm 1} \delta(x - x_0), \tag{3}$$

where $\delta(\cdot)$ is the Dirac δ -function. The absorbing boundary conditions read

$$P_+(x \rightarrow x_A, t|x_0, \sigma_j) = 0, \tag{4a}$$

$$P_-(x \rightarrow x_B, t|x_0, \sigma_j) = 0. \tag{4b}$$

The total PDF to find the particle in x at time t irrespective of its current direction is

$$P(x, t|x_0, \sigma_j) = P_+(x, t|x_0, \sigma_j) + P_-(x, t|x_0, \sigma_j). \tag{5}$$

The corresponding probability flux $J(x, t|x_0, \sigma_j)$ for right-moves and left-moves can be written as

$$J(x, t|x_0, \sigma_j) = v [P_+(x, t|x_0, \sigma_j) - P_-(x, t|x_0, \sigma_j)]. \tag{6}$$

Hence, the total probability flux is

$$J(x, t|x_0) = J(x, t|x_0, +1) + J(x, t|x_0, -1). \tag{7}$$

A. Transient probability density function

In order to calculate the transition path time distribution of RTPs, we need to solve the transient solution of Eq. (2). In this paper, we adopt the derivation method presented in Ref. 44 and generalize the results there. Compared with the transient solution in Ref. 44, our results can change the boundary values of the transition path region arbitrarily, so that we can subsequently explore the parametric dependence of the transition path dynamics of RTPs directly. The detailed derivation is presented in Appendix A.

For the transition region $[x_A, x_B]$, we obtain the explicit results

$$\begin{aligned} P_+(x, t|x_0, +1) &= e^{-\gamma t} \delta(x - x_0 - vt) + \frac{e^{-\gamma t}}{2v} \left[\mathcal{M}_\alpha^0(|x_0 - x|, t) \right. \\ &\quad - \mathcal{M}_\alpha^{\frac{1+\alpha}{2}}(x_0 + x - 2x_A, t) - \mathcal{M}_\alpha^{\frac{1+\alpha}{2}}(2x_B - x_0 - x, t) \\ &\quad \left. + \mathcal{M}_\alpha^{1+\alpha}(2x_B - 2x_A - |x_0 - x|, t) \right] \end{aligned} \tag{8}$$

and

$$\begin{aligned} P_-(x, t|x_0, +1) &= \frac{\gamma^2 e^{-\gamma t}}{2v} \left[\mathcal{N}_0(|x_0 - x|, t) - \mathcal{N}_0(2x_B - x_0 - x, t) \right. \\ &\quad \left. - \mathcal{N}_1(x_0 + x - 2x_A, t) + \mathcal{N}_1(2x_B - 2x_A - |x_0 - x|, t) \right], \end{aligned} \tag{9}$$

where

$$\begin{aligned} \mathcal{M}_\alpha^m(x, t) &= \sum_{n=0}^{\infty} \frac{\gamma}{2} \left[f_{2n+2m-1}(x + 2n(x_B - x_A)) \left\{ 1 + \alpha \frac{x + 2n(x_B - x_A)}{vt + x + 2n(x_B - x_A)} \right\} \right. \\ &\quad \left. + f_{2n+2m+1}(x + 2n(x_B - x_A)) \left\{ 1 + \alpha \frac{x + 2n(x_B - x_A)}{vt - x - 2n(x_B - x_A)} \right\} \right. \\ &\quad \left. + \frac{4\alpha t(n+m)}{\gamma t^2 - \gamma \frac{(x+2n(x_B-x_A))^2}{v^2}} f_{2n+2m}(x + 2n(x_B - x_A), t) \right] \end{aligned} \tag{10}$$

and

$$\begin{aligned} \mathcal{M}_\alpha^0(x, t) = & \sum_{n=0}^{\infty} \frac{\gamma}{2} \left[f_{2n+1}(x + 2(n+1)(x_B - x_A)) \left\{ 1 + \alpha \frac{x + 2(n+1)(x_B - x_A)}{vt + x + 2(n+1)(x_B - x_A)} \right\} \right. \\ & + f_{2n+3}(x + 2(n+1)(x_B - x_A)) \left\{ 1 + \alpha \frac{x + 2(n+1)(x_B - x_A)}{vt - x - 2(n+1)(x_B - x_A)} \right\} \\ & \left. + \frac{4\alpha nt}{\gamma t^2 - \gamma \frac{(x+2n(x_B-x_A))^2}{v^2}} f_{2n+2m}(x + 2n(x_B - x_A), t) + \gamma \frac{t + \alpha \frac{x}{v}}{t - \frac{x}{v}} f_1(x, t) \right], \end{aligned} \tag{11}$$

where $\alpha = \text{sign}(x - x_0) = 1$ if $x > x_0$, and otherwise $\alpha = -1$.

We defined the shorthand notation

$$\mathcal{N}_m(x, t) = \sum_{n=0}^{\infty} f_{2n+2m}(x + 2n(x_B - x_A), t), \quad m \geq 0, \tag{12}$$

and $f_m(x, t)$ is given by

$$f_m(x, t) = \left(\frac{vt - x}{vt + x} \right)^{\frac{m}{2}} I_m \left(\frac{\gamma}{v} \sqrt{v^2 t^2 - x^2} \right) \theta(vt - x). \tag{13}$$

Here, $\theta(x)$ is the Heaviside theta function and $I_m(x, t)$ is the modified Bessel function of the first kind.

These expressions define the transient PDFs $P_{\pm}(x, t|x_0, \pm 1)$ of RTPs with different initial particle velocities.

B. Distribution of transition path time

The forward transition path time distribution $\rho(t)$ is related to the probability flux in the form⁷⁵

$$\rho(t) = \lim_{\theta \rightarrow 0} \frac{J(x_B, t|x_A + \theta)}{\int_0^\infty J(x_B, t|x_A + \theta) dt}. \tag{14}$$

Subsequently, combining Eq. (6) and the boundary conditions (4), we arrive at the relation

$$\begin{aligned} J(x_B, t|x_A, \sigma_j) &= v[P_+(x_B, t|x_A, \sigma_j) - P_-(x_B, t|x_A, \sigma_j)] \\ &= vP_+(x_B, t|x_A, \sigma_j), \end{aligned} \tag{15}$$

for the flux. Therefore, the theoretical solution of $\rho(t)$ can be derived from Eq. (14). The reverse transition path time distribution can be considered analogously and will not be repeated here.

C. Splitting probability

For the calculation of the transition path times for RTPs, we first consider the splitting probabilities $\phi_A(x_0)$ and $\phi_B(x_0)$ of an RTP particle.⁸⁵ $\phi_{A/B}(x_0)$ is the probability that the particle starts from x_0 and escapes the interval $[x_A, x_B]$ through $x_{A/B}$ before touching $x_{B/A}$. The calculations of $\phi_{A/B}(x_0)$ start from the distribution of the first passage time of the particle. Here, we define $K(x_{A/B}, t|x_0, \sigma_j)$ as the first passage time distribution of a particle that is initially in $x_0 \in [x_A, x_B]$ with “right-moving” ($\sigma_j = +1$) and “left-moving” ($\sigma_j = -1$) states, for reaching $x_{A/B}$. $K(x_{A/B}, t|x_0) = \frac{1}{2}[K(x_{A/B}, t|x_0,$

$+1) + K(x_{A/B}, t|x_0, -1)]$ is the first passage time distribution when the particle is initially located in x_0 . We also define $K^{(n)}(x_{A/B}|x_0, \sigma_j)$ as the n th moment of the first passage time distribution when the particle is initially located in x_0 with state σ_j . Then, $K^{(n)}(x_{A/B}|x_0) = \frac{1}{2}[K^{(n)}(x_{A/B}|x_0, +1) + K^{(n)}(x_{A/B}|x_0, -1)]$ is the n th moment of the first passage time distribution when the particle is initially located in x_0 . Meanwhile, the n th moment of the first passage time distribution $K^{(n)}(x_{A/B}|x_0)$ is defined as⁵⁴

$$K^{(n)}(x_{A/B}|x_0) = \int_0^\infty t^n K(x_{A/B}, t|x_0) dt. \tag{16}$$

Then, $K^{(n-1)}(x_{A/B}|x_0, \sigma_j)$ satisfy the coupled backward equations

$$\begin{aligned} -nK^{(n-1)}(x_{A/B}|x_0, +1) &= v \frac{\partial}{\partial x_0} K^{(n)}(x_{A/B}|x_0, +1) \\ &+ \gamma [K^{(n)}(x_{A/B}|x_0, -1) - K^{(n)}(x_{A/B}|x_0, +1)], \end{aligned} \tag{17}$$

$$\begin{aligned} -nK^{(n-1)}(x_{A/B}|x_0, -1) &= -v \frac{\partial}{\partial x_0} K^{(n)}(x_{A/B}|x_0, -1) \\ &+ \gamma [K^{(n)}(x_{A/B}|x_0, +1) - K^{(n)}(x_{A/B}|x_0, -1)], \end{aligned}$$

with the boundary conditions $K(x_A, t|x_A, -1) = K(x_A, t|x_B, +1) = 0$ and $K(x_B, t|x_B, +1) = K(x_B, t|x_A, -1) = 0$. It results to $K^{(n)}(x_A|x_A, -1) = K^{(n)}(x_A|x_B, +1) = 0$ and $K^{(n)}(x_B|x_B, +1) = K^{(n)}(x_B|x_A, -1) = 0$. Moreover, the zeroth moment of first passage time distribution is the so-called splitting probability,

$$\begin{aligned} v \frac{\partial}{\partial x_0} \phi_A^{\sigma_j}(x_0, +1) + \gamma [\phi_A^{\sigma_j}(x_0, -1) - \phi_A^{\sigma_j}(x_0, +1)] &= 0, \\ -v \frac{\partial}{\partial x_0} \phi_A^{\sigma_j}(x_0, -1) + \gamma [\phi_A^{\sigma_j}(x_0, +1) - \phi_A^{\sigma_j}(x_0, -1)] &= 0, \end{aligned} \tag{18}$$

where $\sigma_j = \pm 1$, $\phi_A^{\sigma_j}(x_0, +1)$ and $\phi_A^{\sigma_j}(x_0, -1)$ denote the probabilities for a particle to exit through the left boundary x_A in the σ_j -moving state, given it was initially at position $x_0 \in [x_A, x_B]$ in the “right-moving” and “left-moving” states, respectively. The boundary conditions are

$$\begin{aligned} \phi_A^{+1}(x_A, -1) = 1, \phi_A^{+1}(x_B, +1) = 0, \\ \phi_A^{-1}(x_A, -1) = 1, \phi_A^{-1}(x_B, +1) = 0. \end{aligned} \tag{19}$$

Next, we define $\phi_B^{\sigma_j}(x_0, +1)$ and $\phi_B^{\sigma_j}(x_0, -1)$ as the splitting probabilities of exiting through the right boundary x_B when initially in the right and left-moving states, respectively. Similarly, $\phi_B^{\sigma_j}(x_0, +1)$ and $\phi_B^{\sigma_j}(x_0, -1)$ satisfy the coupled equations

$$\begin{aligned} v \frac{\partial}{\partial x_0} \phi_B^{\sigma_j}(x_0, +1) + \gamma [\phi_B^{\sigma_j}(x_0, -1) - \phi_B^{\sigma_j}(x_0, +1)] &= 0, \\ -v \frac{\partial}{\partial x_0} \phi_B^{\sigma_j}(x_0, -1) + \gamma [\phi_B^{\sigma_j}(x_0, +1) - \phi_B^{\sigma_j}(x_0, -1)] &= 0, \end{aligned} \tag{20}$$

where $\phi_B^{+1}(x_A, -1) = 0$, $\phi_B^{+1}(x_B, +1) = 1$, $\phi_B^{-1}(x_A, -1) = 0$, and $\phi_B^{-1}(x_B, +1) = 1$. Hence, the splitting probabilities of a particle to exit through the right or left boundary given $x_0 \in [x_A, x_B]$ are $\phi_A(x_0, \pm 1) = [\phi_A^{+1}(x_0, \pm 1) + \phi_A^{-1}(x_0, \pm 1)]/2$ and $\phi_B(x_0, \pm 1) = [\phi_B^{+1}(x_0, \pm 1) + \phi_B^{-1}(x_0, \pm 1)]/2$, respectively.

For the boundary conditions (19), we solve Eq. (18). Let $\psi^{\sigma_j}(x_0) = \phi_A^{\sigma_j}(x_0, +1) + \phi_A^{\sigma_j}(x_0, -1)$ and $\mu^{\sigma_j}(x_0) = \phi_A^{\sigma_j}(x_0, -1) - \phi_A^{\sigma_j}(x_0, +1)$. Therefore, Eq. (18) can be rewritten as

$$\begin{aligned} v \frac{\partial}{\partial x_0} \mu^{\sigma_j}(x_0) &= 0, \\ v \frac{\partial}{\partial x_0} \psi^{\sigma_j}(x_0) + 2\gamma \mu^{\sigma_j}(x_0) &= 0. \end{aligned} \tag{21}$$

Then, with the help of Eq. (19), we find

$$\begin{aligned} \phi_A^{-1}(x_0, +1) &= \frac{\gamma(x_B - x_0)}{v + \gamma(x_B - x_A)}, \\ \phi_A^{-1}(x_0, -1) &= -\frac{\gamma(x_0 - x_A)}{v + \gamma(x_B - x_A)} + 1, \\ \phi_A^{+1}(x_0, +1) &= \frac{\gamma(x_B - x_0)}{v + \gamma(x_B - x_A)}, \\ \phi_A^{+1}(x_0, -1) &= -\frac{\gamma(x_0 - x_A)}{v + \gamma(x_B - x_A)} + 1. \end{aligned} \tag{22}$$

Equation (20) can be also solved using the same strategy, resulting in

$$\begin{aligned} \phi_B^{-1}(x_0, +1) &= \frac{\gamma(x_0 - x_A) + v}{v + \gamma(x_B - x_A)}, \phi_B^{-1}(x_0, -1) = \frac{\gamma(x_0 - x_A)}{v + \gamma(x_B - x_A)}, \\ \phi_B^{+1}(x_0, +1) &= \frac{\gamma(x_0 - x_A) + v}{v + \gamma(x_B - x_A)}, \phi_B^{+1}(x_0, -1) = \frac{\gamma(x_0 - x_A)}{v + \gamma(x_B - x_A)}. \end{aligned} \tag{23}$$

Finally, the splitting probabilities of the RTP to exit through x_A and x_B are given by

$$\begin{aligned} \phi_A(x_0) &= \frac{1}{2} [\phi_A(x_0, +1) + \phi_A(x_0, -1)] = \frac{1}{2} \frac{2\gamma(x_B - x_0) + v}{v + \gamma(x_B - x_A)}, \\ \phi_B(x_0) &= \frac{1}{2} [\phi_B(x_0, +1) + \phi_B(x_0, -1)] = \frac{1}{2} \frac{2\gamma(x_0 - x_A) + v}{v + \gamma(x_B - x_A)}. \end{aligned} \tag{24}$$

D. Mean transition path time and coefficient of variation

We define $\tau^{\text{TP}}(x_B|x_A)$ and $\tau^{\text{TP}}(x_A|x_B)$ as the mean transition path times of the particle from $x_{A/B}$ to $x_{B/A}$. Moreover, $\tau^{\text{TP}}(x_B|x_A)$ and $\tau^{\text{TP}}(x_A|x_B)$ are called the positive/negative direction mean transition path times, respectively. According to Eq. (17), the first moments of the first passage time distribution $K^{(1)}(x_{A/B}|x_0, \pm 1)$ satisfy the coupled backward equations⁵⁴

$$\begin{aligned} v \frac{\partial}{\partial x_0} K^{(1)}(x_{A/B}|x_0, +1) + \gamma [K^{(1)}(x_{A/B}|x_0, -1) - K^{(1)}(x_{A/B}|x_0, +1)] &= -\phi_{A/B}(x_0, +1), \\ -v \frac{\partial}{\partial x_0} K^{(1)}(x_{A/B}|x_0, -1) + \gamma [K^{(1)}(x_{A/B}|x_0, +1) - K^{(1)}(x_{A/B}|x_0, -1)] &= -\phi_{A/B}(x_0, -1). \end{aligned} \tag{25}$$

Here, we provide the calculations for $K^{(1)}(x_B|x_0, \pm 1)$; $K^{(1)}(x_A|x_0, \pm 1)$ can be calculated analogously. A specific form of $K^{(1)}(x_A|x_0, \pm 1)$ is presented in Appendix B. Define $\eta(x_0) = K^{(1)}(x_B|x_0, +1) + K^{(1)}(x_B|x_0, -1)$ and further $\epsilon(x_0) = K^{(1)}(x_B|x_0, +1) - K^{(1)}(x_B|x_0, -1)$. We then find

$$v \frac{\partial}{\partial x_0} \epsilon(x_0) = -2\phi_B(x_0), \tag{26}$$

$$v \frac{\partial}{\partial x_0} \eta(x_0) - 2\gamma \epsilon(x_0) = \phi_B(x_0, -1) - \phi_B(x_0, +1).$$

Together with the boundary conditions, we obtain

$$\epsilon(x_0) = \frac{2}{v} \int_{x_0}^{x_B} \phi_B(y) dy + C_1, \tag{27}$$

$$\begin{aligned} \eta(x_0) &= \frac{4\gamma}{v^2} \int_{x_A}^{x_0} \int_y^{x_B} \phi_B(z) dz dy + \frac{2\gamma}{v} C_1(x_0 - x_A) \\ &+ \frac{1}{v} \int_{x_A}^{x_0} \phi_B(y, -1) dy - \frac{1}{v} \int_{x_A}^{x_0} \phi_B(y, +1) dy + C_2, \end{aligned}$$

where

$$\begin{aligned} C_1 &= -\frac{v}{\gamma(x_B - x_A) + v} \left[\frac{2\gamma}{v^2} \int_{x_A}^{x_B} \int_y^{x_B} \phi_B(z) dz dy \right. \\ &+ \frac{1}{2v} \int_{x_A}^{x_B} \phi_B(y, -1) dy - \frac{1}{2v} \int_{x_A}^{x_B} \phi_B(y, +1) dy \\ &\left. + \frac{1}{v} \int_{x_A}^{x_B} \phi_B(y) dy \right], \\ C_2 &= C_1 + \frac{2}{v} \int_{x_A}^{x_B} \phi_B(y) dy. \end{aligned} \tag{28}$$

Then, we arrive at the solution $K^{(1)}(x_B|x_0, \pm 1) = \frac{1}{2} [\eta(x_0) \pm \epsilon(x_0)]$.

According to $K^{(1)}(x_{A/B}|x_0) = \frac{1}{2} [K^{(1)}(x_{A/B}|x_0, +1) + K^{(1)}(x_{A/B}|x_0, -1)]$, the mean first passage time after normalization is

given by

$$\tau^{\text{FP}}(x_{A/B}|x_0) = \frac{K^{(1)}(x_{A/B}|x_0)}{\phi_{A/B}(x_0)}, \quad (29)$$

where $\tau^{\text{FP}}(x_{A/B}|x_0)$ is the mean first passage time of the particle from x_0 to $x_{A/B}$.

Hence, $\tau^{\text{FP}}(x_{B/A}|x_{A/B})$ are the mean first passage times of the particle from $x_{A/B}$ to $x_{B/A}$, respectively. Considering that x_A and x_B are two absorbing boundaries, the mean transition path times are consequently given by

$$\begin{aligned} \tau^{\text{TP}}(x_B|x_A) &= \tau^{\text{FP}}(x_B|x_0 \rightarrow x_A), \\ \tau^{\text{TP}}(x_A|x_B) &= \tau^{\text{FP}}(x_A|x_0 \rightarrow x_B). \end{aligned} \quad (30)$$

Therefore, when $x_{A/B}$ are absorbing boundaries, the mean transition path time can be obtained from the mean first passage time with the help of Eq. (30), i.e.,

$$\begin{aligned} \tau^{\text{TP}}(x_B|x_A) &= \frac{K^{(1)}(x_B|x_A)}{\phi_B(x_A)} = \frac{C_2}{2\phi_B(x_A)}, \\ \tau^{\text{TP}}(x_A|x_B) &= \frac{K^{(1)}(x_A|x_B)}{\phi_A(x_B)} = \frac{N_2}{2\phi_A(x_B)}, \end{aligned} \quad (31)$$

where the further simplifications of C_2 and N_2 are presented in Appendix B.

The second moment of the first passage time distribution, $K^{(2)}(x_{A/B}|x_0, \pm 1)$ can also be derived from Eq. (17), for which the detailed calculations are presented in Appendix C. Moreover, to investigate the transition path time distribution in more detail, we also consider the coefficient of variation C_V of the transition path

time distribution. C_V has the form⁴⁹

$$C_V = \frac{1}{\langle t_{\text{TP}} \rangle} \left(\langle t_{\text{TP}}^2 \rangle - \langle t_{\text{TP}} \rangle^2 \right)^{1/2}, \quad (32)$$

where $\langle t_{\text{TP}}^2 \rangle$ is the second moment of the transition path time distribution, given by $\langle t_{\text{TP}}^2 \rangle = \frac{K^{(2)}(x_{B/A}|x_{A/B})}{\phi_{B/A}(x_{A/B})}$, and $\langle t_{\text{TP}} \rangle = \tau^{\text{TP}}(x_{B/A}|x_{A/B})$.

E. Mean transition path shape

We define $\tau_{\text{shape}}^{\text{TP}}(x_0|x_{A/B})$ as the mean transition path shape of particles from $x_{A/B}$ to x_0 , respectively. These quantities are obtained from the relations⁵⁴

$$\begin{aligned} \tau_{\text{shape}}^{\text{TP}}(x_0|x_A) &= \tau^{\text{FP}}(x_A|x_0), \\ \tau_{\text{shape}}^{\text{TP}}(x_0|x_B) &= \tau^{\text{FP}}(x_B|x_0). \end{aligned} \quad (33)$$

Combined with Eq. (30), one obtains the results for the mean transition path shape for RTPs.

III. ALGORITHM FOR DICHOTOMOUS NOISE

We here focus on generating dichotomous noise $\sigma(t)$ ⁸⁶ and include this in Eq. (1). When the parameters of dichotomous noise are determined, dichotomous noise can be generated from the corresponding simulation algorithm.

Suppose that the time period $[0, t]$ is divided into n equal parts, $\{t_0, t_1, t_2, \dots, t_n\}$. We then generate the sequence $\{\sigma(t_0), \sigma(t_1), \sigma(t_2), \dots, \sigma(t_n)\}$ of the dichotomous noise, following the procedure: first, the initial state of the dichotomous noise is assumed to be $\sigma(t_0) = a$ or $\sigma(t_0) = b$. We then generate a sequence of random numbers, $\{R_i, i = 0, 1, 2, \dots\}$ corresponding to a uniform

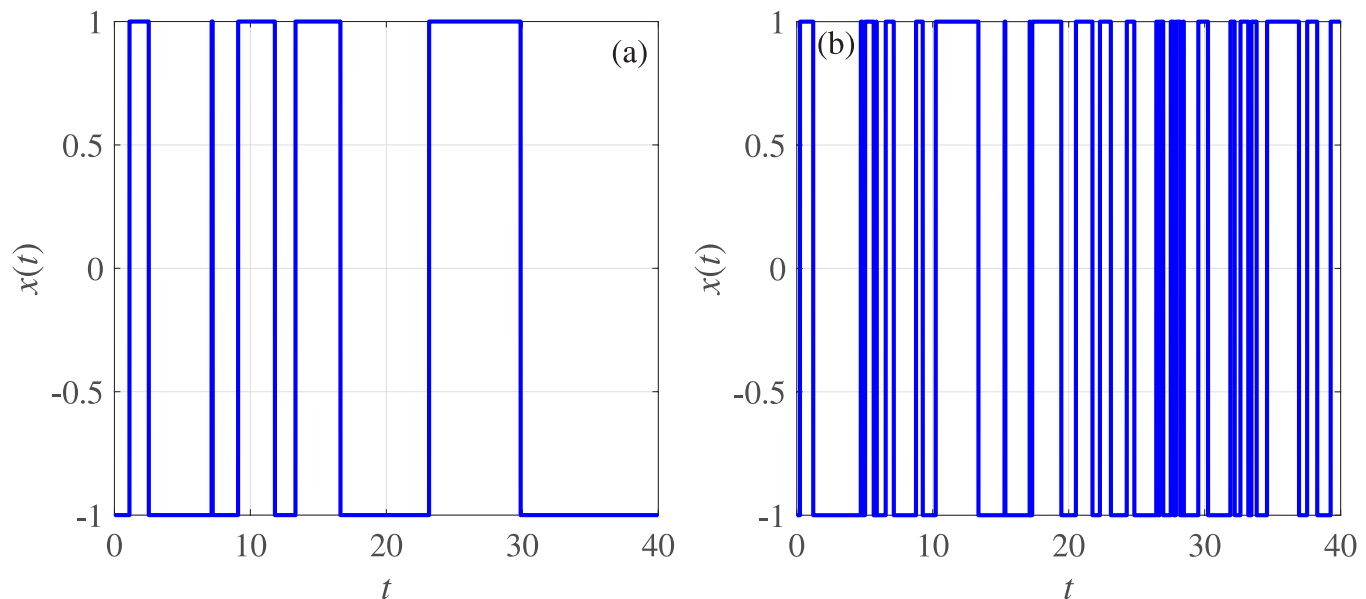


FIG. 1. Sample paths of the dichotomous noise $\sigma(t)$ for two different values of parameter γ . (a) $\gamma = 0.25$, (b) $\gamma = 1.0$.

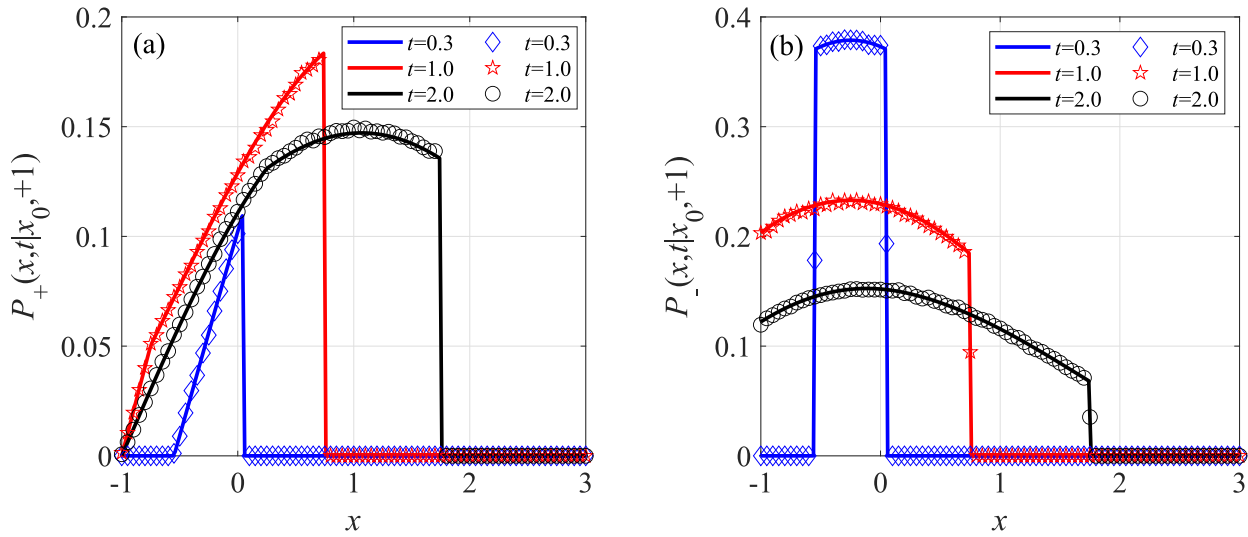


FIG. 2. Transient probability density function $P_{\pm}(x, t|x_0, +1)$ for three different times t of particles in the transition region $[-1, 3]$ with $x_0 = -0.25$, $\gamma = 1.0$, and $\nu = 1.0$. The solid lines represent the theoretical results of Eqs. (8) and (9), and the symbols represent the Monte Carlo results.

distribution on the interval $[0, 1]$. Suppose further that p_{aa}, p_{ba} are the probabilities that the state of the particle switches from a to a , and b to a , respectively. Subsequently, we compare the difference between R_i, p_{aa} , and p_{ba} . As presented in Ref. 86, p_{aa} and p_{ba} are given by

$$\begin{aligned} p_{aa} &= \frac{1}{2} + \frac{1}{2} \exp\left(-\frac{1}{2}\Delta t\right), \\ p_{ba} &= \frac{1}{2} - \frac{1}{2} \exp\left(-\frac{1}{2}\Delta t\right), \end{aligned} \tag{34}$$

where Δt is time step of the simulation. Here, we choose $a = 1$ and $b = -1$.

For the case of $\sigma(t_0) = a$, if $R_0 < p_{aa}$, we take $\sigma(t_1) = a$, and $\sigma(t_1) = b$ if $R_0 \geq p_{aa}$. For the $\sigma(t_0) = b$ case, if $R_0 < p_{ba}$, we take $\sigma(t_1) = a$, and $\sigma(t_1) = b$ if $R_0 \geq p_{ba}$. Then, if $\sigma(t_1) = a$, we compare the size of R_1 with p_{aa} . If $R_1 < p_{aa}$, we take $\sigma(t_2) = a$, and if $R_1 \geq p_{aa}$, we take $\sigma(t_2) = b$. However, if $\sigma(t_1) = b$, we should compare the size of R_1 with p_{ba} . By repeating this procedure, we obtain the sequence of dichotomous noise $\{\sigma(t_0), \sigma(t_1), \sigma(t_2), \dots, \sigma(t_n)\}$. Different parameters are chosen to obtain varying dichotomous

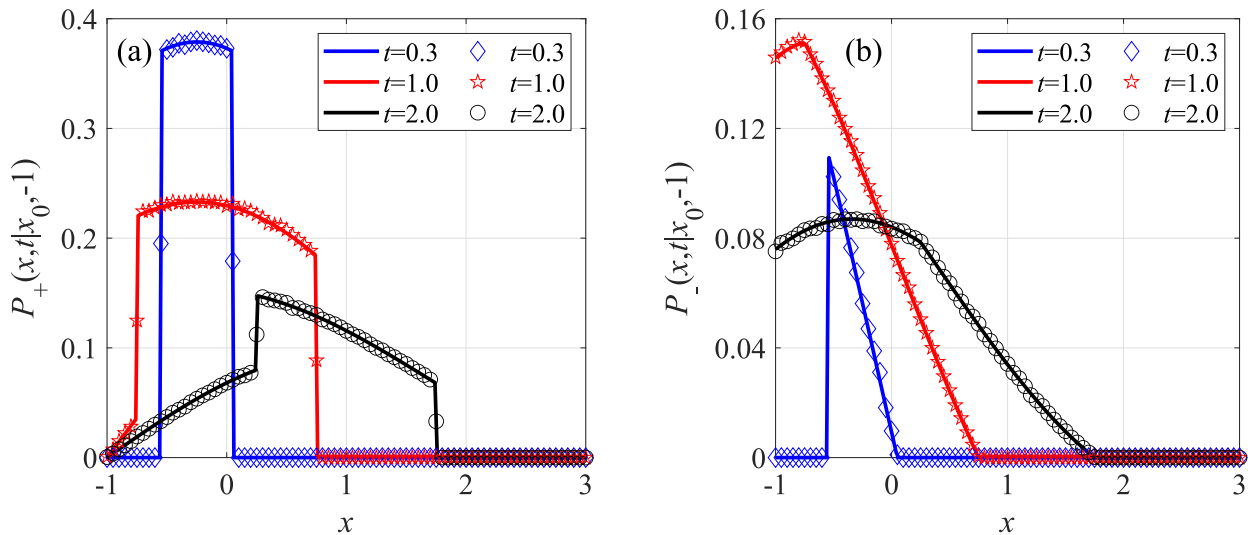


FIG. 3. Transient probability density function $P_{\pm}(x, t|x_0, -1)$ for three different times t of particles in the transition region $[-1, 3]$ with $x_0 = -0.25$, $\gamma = 1.0$, and $\nu = 1.0$. The solid lines represent the analytical results of Eqs. (A8) and (A9), and the symbols represent the Monte Carlo results.

noise sequences, as shown in Fig. 1. We see that as parameter γ is increased, the particle switches more frequently between the states $+1$ and -1 , as expected.

IV. RESULTS

We now employ the framework established so far and consider the transition path properties of RTPs, choosing $[-1, 3]$ as the transition region. The direction for particle moves from -1 to

3 is the forward direction, and 3 to -1 is the reverse direction. Specifically, we present the results for the transient probability density, transition path time distribution, splitting probability, mean transition path time, coefficient of variation, and mean transition path shapes in this transition region. Subsequently, the correctness of the theoretical results of the transition path properties for RTPs is verified by Monte Carlo simulations. We find that both smaller particle velocities v , larger particle tumble rates γ , and the change of the transition path region may lead to an asymmetry

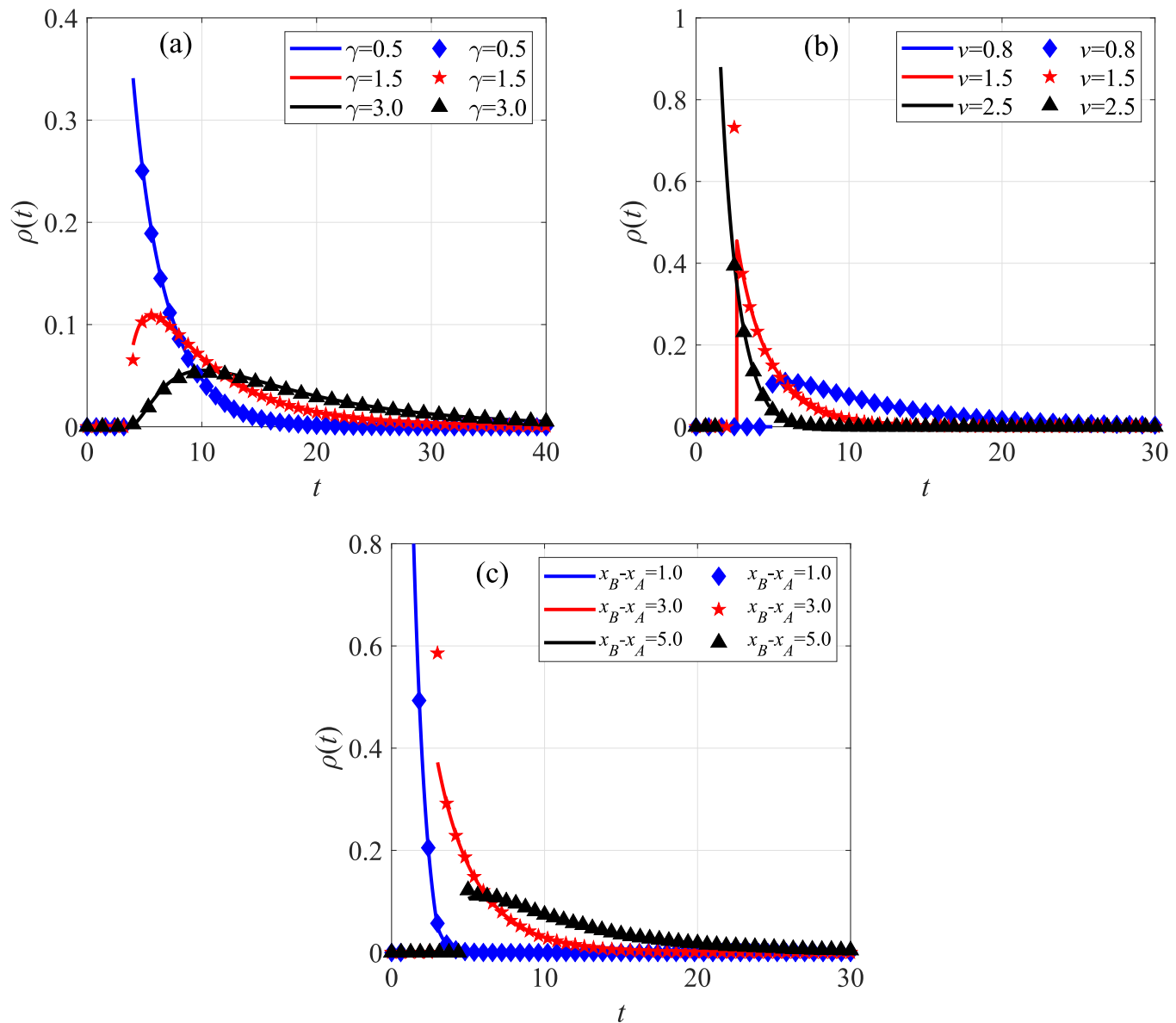


FIG. 4. Transition path time distribution $\rho(t)$ for an RTP with different parameters. The solid lines stand for the analytic expressions (14), while the three different symbols represent the simulations. (a) $\rho(t)$ for different tumble rates γ on the transition region $[-1, 3]$ and for $v = 1.0$. (b) $\rho(t)$ for different particle speeds, transition region $[-1, 3]$, and $\gamma = 1.0$. (c) $\rho(t)$ with $\gamma = 1.0$, $v = 1.0$, $x_A = -1.0$ for three different values of $x_B - x_A$.

of the transition path times and transition path shapes in the two directions.

A. Transient probability density function

We consider the transient probability density functions of RTPs at different time instants and verify the theoretical results of the transient probability density functions by numerical simulations in Figs. 2 and 3. First, it can be seen that our theoretical results very nicely match the simulations results. Moreover, we observe that the transient probability densities of the particles have discontinuous

intermittent points at certain locations in the transition region $[-1, 3]$. For instance, in Fig. 3(a), we see that there is a discontinuity in the transient probability density $P_+(x, t|x_0, -1)$ at $\hat{x} = -0.75$ when $\hat{t} = 1$. According to the dynamics of RTPs, it is possible to reach the left absorbing boundary x_A when the particle is in a “left-moving” state. However, when the initial position of the particle is at x_0 , it needs at least $t_1 = (x_0 - x_A)/v$ to reach x_A . Concurrently, after the particle arrives at x_0 , in a fraction case, the particle will be absorbed by the left absorbing boundary x_A , while some particles will switch to a positive velocity and move away from x_A . Such switches occur when $\gamma \neq 0$. Specifically, this fraction of realizations will

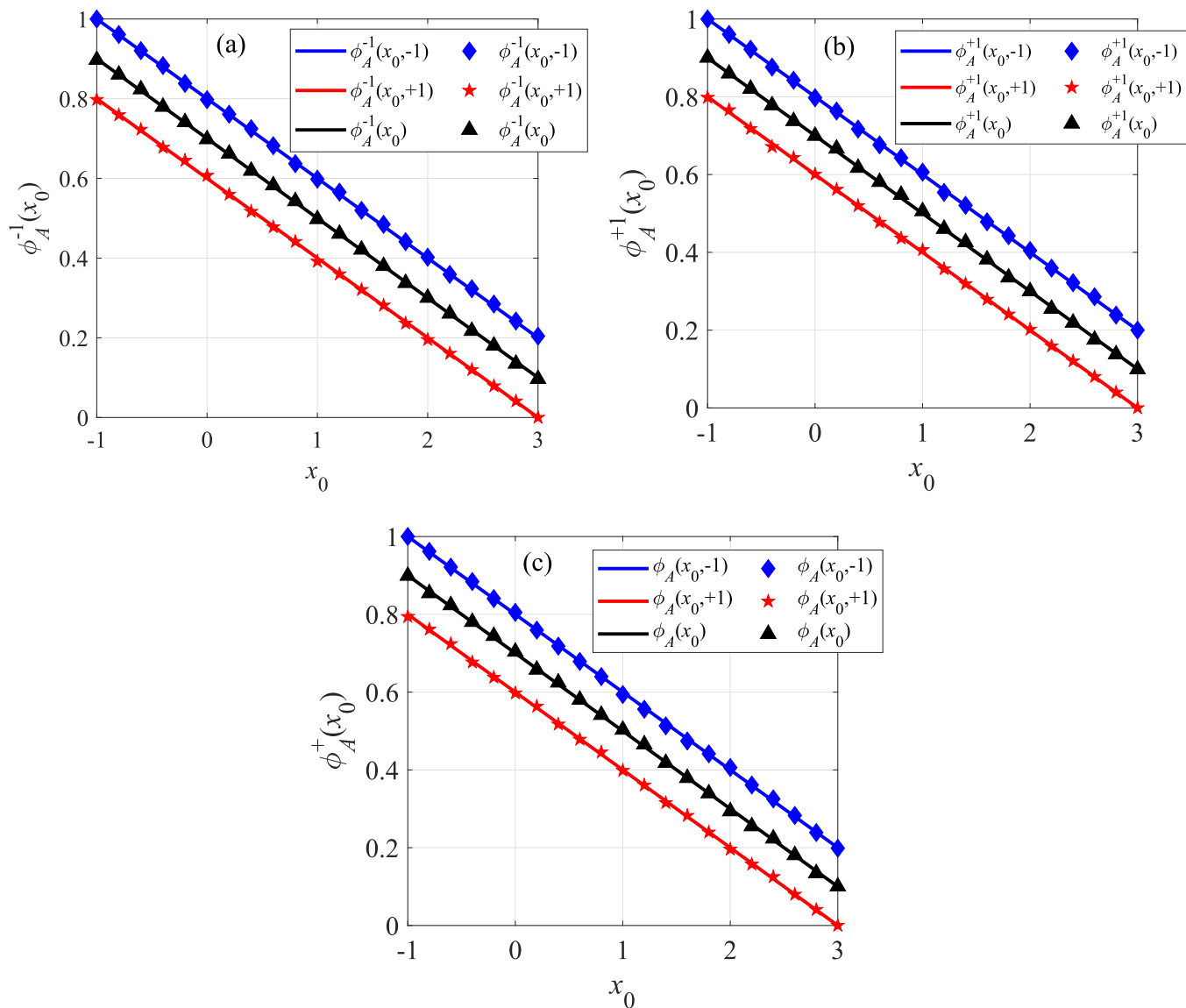


FIG. 5. Splitting probabilities $\phi_A(x_0)$ of particles in a “left-moving” state followed by an exit through the left boundary $x = x_A$. The transition region is $[-1, 3]$, $\gamma = 1.0$, and $v = 1.0$. The solid lines stand for the analytic expressions in Eqs. (22) and (24), the three different symbols represent the simulation data.

move $v(t - t_0)$ to reach $\hat{x} = x_A + v(t - t_1) = 2x_A - x_0 + vt$ during the time period $t - t_1$. This position is exactly the intermittent point presented in the transient probability density function in Fig. 3(a).

We note that it can be observed from the theoretical results of the transient probability density function in Eqs. (A8) and (A9) that the transient probability density $P_{\pm}(x, t|x_0 \rightarrow x_B, -1)$ of the particle is different from 0 when the initial position x_0 converges to the right absorbing boundary x_B and has a negative velocity; whereas, when x_0

converges to the left absorbing boundary x_A with a positive velocity, the transient probability density $P_{\pm}(x, t|x_0 \rightarrow x_B, +1)$ is 0. However, when the initial position x_0 converges to x_A , the transient probability density $P_{\pm}(x, t|x_0 \rightarrow x_A, +1)$ of the particle is different from 0, while for $x_0 \rightarrow x_A$ with a negative velocity, the transient probability density $P_{\pm}(x, t|x_0 \rightarrow x_A, -1)$ is 0. This is also clearly different from Brownian motion, for which the transient probability density of a particle at two absorbing boundaries must be zero in the transition region.

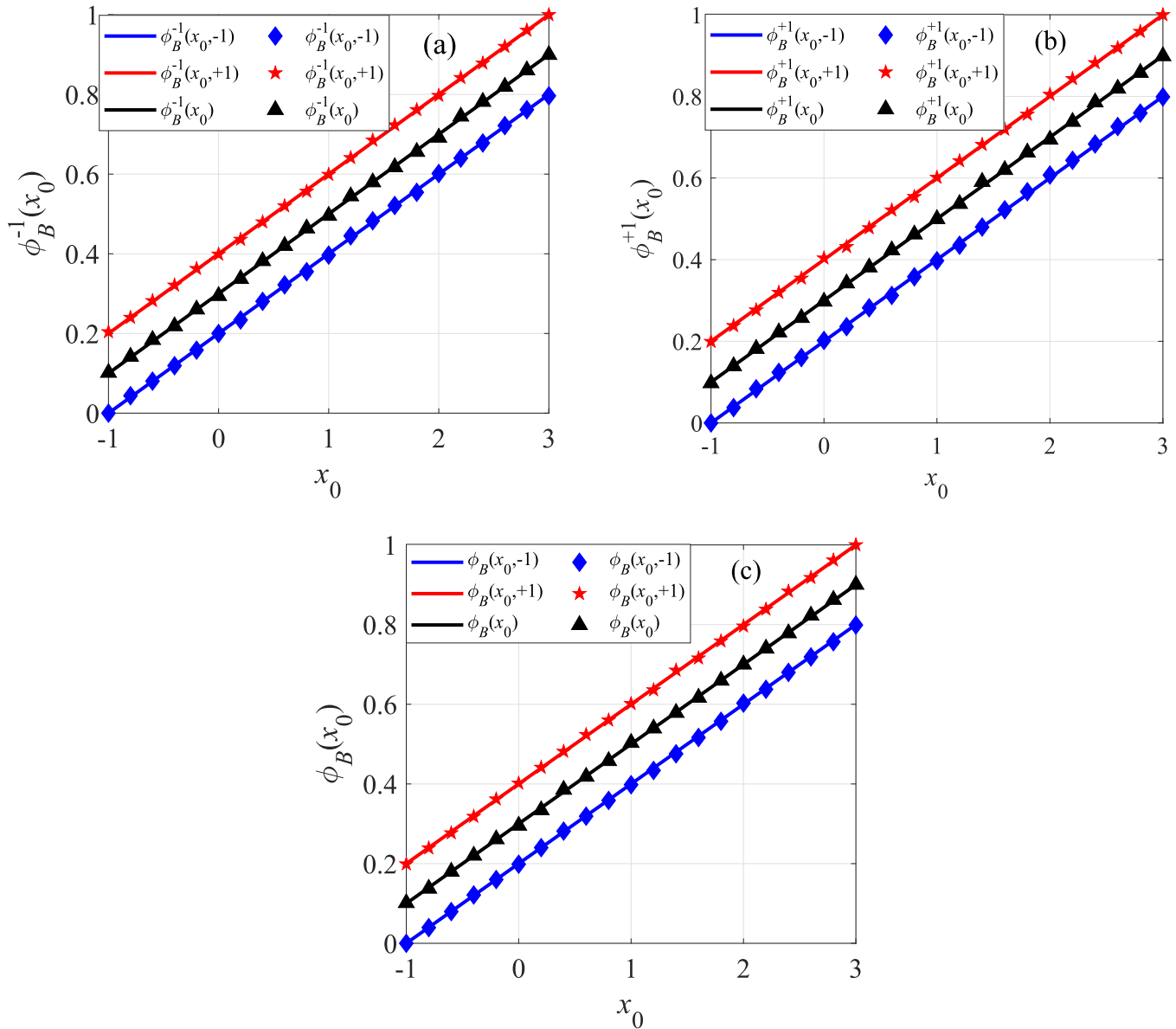


FIG. 6. Splitting probabilities $\phi_B(x_0)$ to observe particles in a right-moving state and exiting from the right boundary $x = x_B$. The transition region is $[-1, 3]$, $\gamma = 1.0$, and $v = 1.0$. The solid lines represent the analytic expressions in Eqs. (23) and (24), the three different symbols represent the simulations data.

B. Transition path time distribution

In this section, the probability flux of the system is obtained mainly based on the transient probability density of run and tumble particles, and thus the transition path time distributions of the particles are calculated. It can be seen from Fig. 4 that the transition path time distribution also has discontinuity points inevitably. We consider the influence of system parameters on the transition path time

distribution of run and tumble particles, and through the comparison of Monte Carlo simulation, it can be found that the fitting effect is also relatively good, and the correctness of the theoretical results of the transition path time distribution given in the paper is verified.

As shown in Fig. 4, the peak of transition path time distribution decreases as the tumble rate γ increases or the speed of particle v decreases. Particularly, according to panels (a) and (b), it can be observed that growing v accelerates the transition of particles to a

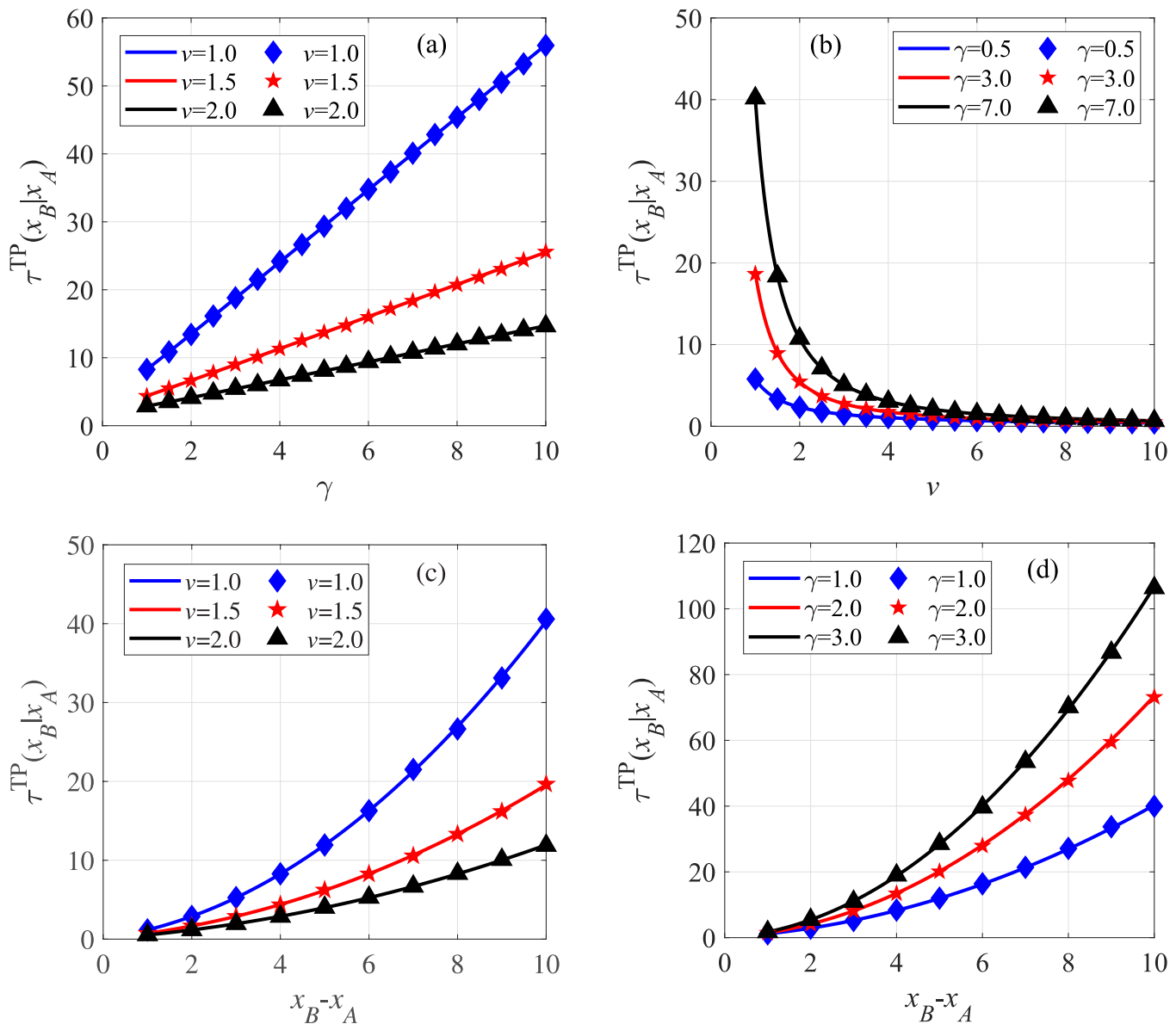


FIG. 7. Forward mean transition path time $\tau^{TP}(x_B|x_A)$ for RTPs for different system parameters. (a) $\tau^{TP}(x_B|x_A)$ as a function of tumbling rate γ for three different values of speed v ($v = 1.0, 1.5,$ and 2.0) on the interval $[-1, 3]$. (b) Variation of $\tau^{TP}(x_B|x_A)$ with v for three different values of γ ($\gamma = 0.5, 3.0,$ and 7.0) on the interval $[-1, 3]$. (c) $\tau^{TP}(x_B|x_A)$ as a function of $x_B - x_A$ for $\gamma = 1.0$ and $x_A = -1$. (d) $\tau^{TP}(x_B|x_A)$ as a function of $x_B - x_A$ for $v = 1.0, x_B = 1.0$. The solid lines stand for the analytic expression (B5), the three different symbols represent the Monte Carlo simulations.

09 May 2025 05:44:22

certain extent, while growing γ delays the transition of particles. If we increase the transition region, the shape of the transition path time distribution becomes wider, as shown in panel (c).

C. The splitting probability

To discuss the transition path time and transition path shape of an RTP, we first consider the splitting probability in the transition region $[-1, 3]$. Figure 5 shows $\phi_A(x_0)$. Comparing Figs. 5(a)

and 5(b), we see that if the particle is initially located at x_0 , the splitting probabilities for leaving the transition region from the left absorbing boundary x_A with either a positive or negative velocity are equal. Concurrently, as shown in Fig. 5, it is more favorable for the particle to escape from the left boundary x_A if the particle is initially located at x_0 and has a negative velocity, as compared to having a positive velocity. Second, if the particle starts at x_0 and escapes from x_A , the splitting probability $\phi_A(x_0)$ with positive and negative velocities are equal. Moreover, the splitting probability of a particle

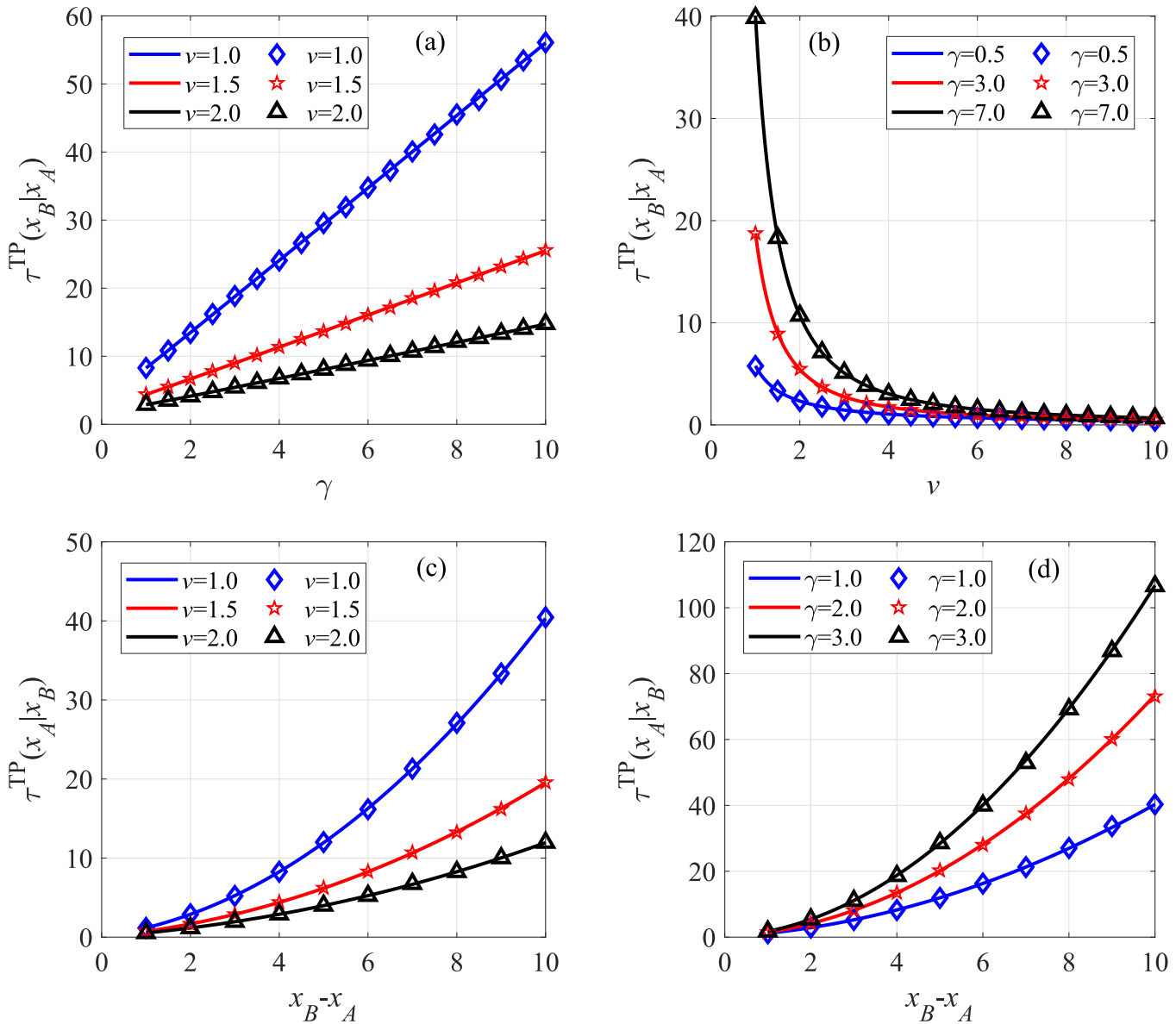


FIG. 8. Reverse mean transition path time $\tau^{\text{TP}}(x_A|x_B)$ for different parameters. (a) Plot of $\tau^{\text{TP}}(x_A|x_B)$ as a function of tumble rate γ for three different values of v . (b) $\tau^{\text{TP}}(x_A|x_B)$ vs v , from Eq. (B6). The transition region in (a) and (b) is chosen as $[-1, 3]$. (c) $\tau^{\text{TP}}(x_A|x_B)$ as a function of $x_B - x_A$ for $\gamma = 1.0$ and $x_A = -1$. (d) $\tau^{\text{TP}}(x_A|x_B)$ as a function of $x_B - x_A$ for $v = 1.0$, $x_B = 1.0$. The solid lines stand for the analytic expression in Eq. (B6), the three different symbols represent the Monte Carlo simulations.

09 May 2025 05:44:22

escaping from the left boundary x_A is not equal to unity when the particle initially has a positive velocity. Similarly, if the particle initially has a negative velocity, the splitting probability differs from 0. Finally, we note that agreement with the Monte Carlo simulations is favorable.

Similarly, Fig. 6 illustrates the splitting probability $\phi_B(x_0)$ for RTPs in the free-diffusion case. First, we note from Figs. 6(a) and 6(b) that the splitting probabilities for escaping from the right boundary x_B with either a positive or negative velocity are equal

when the particle starts from x_0 and has a negative velocity. The same is true if the particle initially has a positive velocity. Second, the comparison reveals that it is more favorable for the particle to escape from x_B when the particle initially has a positive velocity. Moreover, we find that when the particle is initially located at x_A with a positive velocity, the probability of particle escape from x_B is no longer equal to 0. However, if the particle is located at x_B and has a negative velocity, the probability of the particle to escape from x_B is also no longer equal to 1. Finally, we note that, again, our theoretical results match

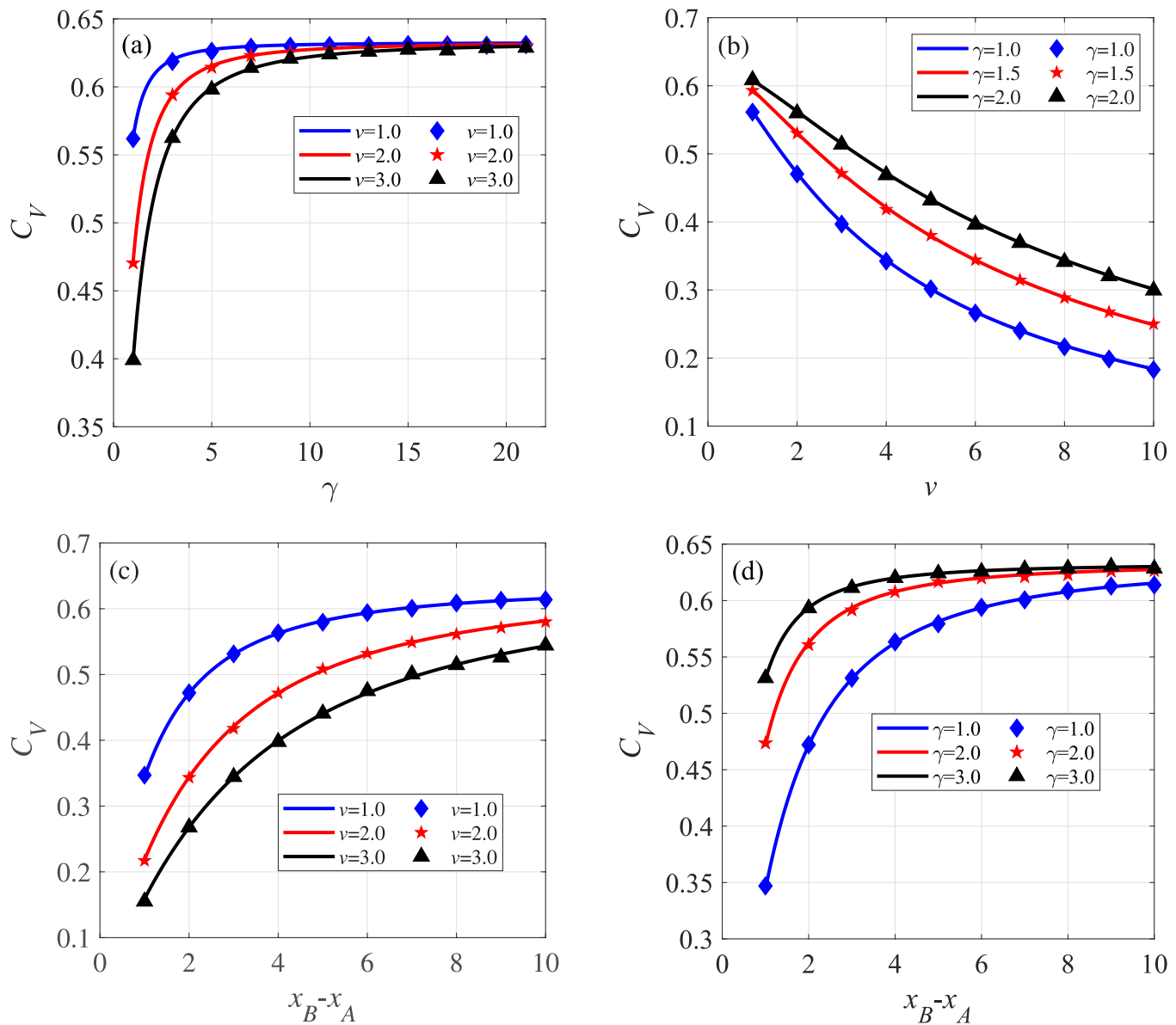


FIG. 9. Coefficient of variation as a function of (a) tumbling rate γ and (b) speed v . In both cases, the transition region is $[-1, 3]$. Coefficient of variation as a function of (c) $x_B - x_A$ for $x_A = -1.0$ and $\gamma = 1.0$; and (d) $x_B - x_A$ for $x_B = 1.0$ and $v = 1.0$. The lines represent the analytical results from Eq. (32), the symbols represent the Monte Carlo simulations.

09 May 2025 05:44:22

the Monte Carlo simulations. Combining Figs. 5 and 6, we find that $\phi_A(x_0) + \phi_B(x_0) = 1$ is still satisfied for RTPs.

D. Mean transition path time and coefficient of variation

We proceed with the transition path times in the two directions. Figure 7 demonstrates the effect of system parameters on the forward mean transition path time $\tau^{\text{TP}}(x_B|x_A)$ for RTPs.

As can be seen from panel (a), $\tau^{\text{TP}}(x_B|x_A)$ is decreasing as the particle speed of v increases, and when v is given, $\tau^{\text{TP}}(x_B|x_A)$ increases linearly with the particle tumble rate γ . As shown in panel (b), $\tau^{\text{TP}}(x_B|x_A)$ increases as γ gets larger. If we increase the transition path region, $\tau^{\text{TP}}(x_B|x_A)$ also increases. It is worth noting that we found that when $x_B - x_A$ and $x_A(x_B)$ are determined, the forward transition path time is independent of the value of $x_A(x_B)$. Again, the Monte Carlo simulations show nice agreement.

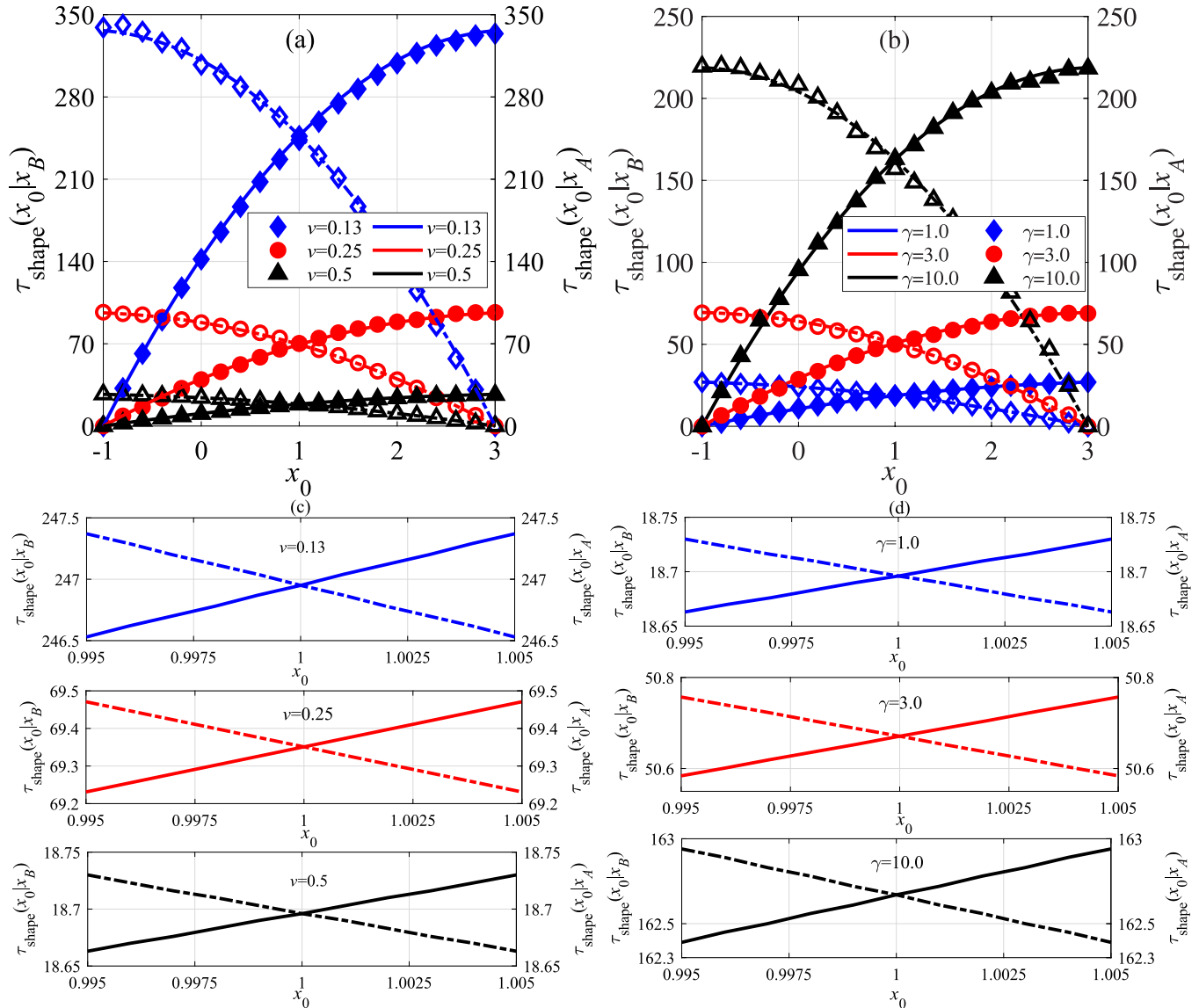


FIG. 10. Mean transition path shape $\tau_{\text{shape}}^{\text{TP}}(x_B|x_A)$ and $\tau_{\text{shape}}^{\text{TP}}(x_A|x_B)$ (a) for different particle speeds v with $\gamma = 1.0$ and $[-1, 3]$, and (b) for different tumble rates γ , where $v = 0.5$ and $[-1, 3]$. (c) and (d) Theoretical results of the mean transition path shape for the two transition directions. Symbols represent simulations, the lines represent the theoretical results (33), (B8), and (B9).

Figure 8 shows the effect of system parameters on the reverse transition path time $\tau^{\text{TP}}(x_A|x_B)$. From panel (a), we see that $\tau^{\text{TP}}(x_A|x_B)$ exhibits a linear growth with γ . As ν increases, $\tau^{\text{TP}}(x_A|x_B)$ decreases, as shown in panel (b). When we decrease the length of the transition region, $\tau^{\text{TP}}(x_A|x_B)$ also decreases, as expected.

In Appendix B, we derive the analytic expression (B7), proving theoretically that the forward transition path time $\tau^{\text{TP}}(x_B|x_A)$ is equal to the reverse transition path time $\tau^{\text{TP}}(x_A|x_B)$. We conclude that the transition path times of RTPs in the two directions are symmetric, analogous to the behavior of Brownian motion.⁷⁰

We also see that the coefficient of variation C_V for the transition path time distribution in both directions are less than 1. Particularly, we show the effect of system parameters on C_V in the forward direction; the reverse case can be similarly assessed. Generally, the results for C_V demonstrate that the transition path time distribution is relatively focused, i.e., the standard deviation is smaller than the mean.

Figure 9(a) shows that C_V gradually increases with the growing tumble rate γ and flattens out when γ roughly exceeds 10. C_V decreases with growing ν and x_A , and it increases with growing x_B . The variations with x_A and x_B reflect the varying size of the transition region. From comparison with Fig. 4, we see that the shape of the transition path time distribution $\rho(t)$ widens with the increase of γ or $x_B - x_A$, as shown in panels (a) and (c); these correspond to a larger C_V . From panel (b), we see that the shape of $\rho(t)$ is narrower when ν is larger, and thus C_V decreases. As the width of $\rho(t)$ increases, the peak of $\rho(t)$ decreases, as expected. Thus, C_V increases with growing γ and the transition region, while it decreases with ν .

E. Mean transition path shape

Finally, we consider the effects of particle speed ν and tumble rate γ on the mean transition path shapes $\tau_{\text{shape}}^{\text{TP}}(x_B|x_A)$ and $\tau_{\text{shape}}^{\text{TP}}(x_A|x_B)$ in two directions on the transition path region $[-1, 3]$. In Fig. 10, panels (a) and (b) demonstrate that as ν increases or γ decreases, the mean transition path shapes in both directions tend to decrease gradually. In particular, we also examine the effects of ν and γ on the symmetry of the transition path shape. As shown in panels (c) and (d), ν and γ cannot affect the asymmetry of the transition path shapes. We note that, again, the numerical and theoretical results are in good agreement with each other. The proof that the transition path shapes $\tau_{\text{shape}}^{\text{TP}}(x_0|x_B)$ and $\tau_{\text{shape}}^{\text{TP}}(x_0|x_A)$ are equal with respect to the transition path interval $[x_A, x_B]$ is presented in Appendix B.

V. CONCLUSIONS

We presented the analytic and simulation results for the transition path dynamics of RTPs in the free-diffusion case. Particularly, the results for the transient probability density function, transition path time distribution, splitting probability, transition path time, and transition path shape are considered. The theoretical results are compared to the Monte Carlo simulations, that in all cases show nice agreement. From our results, we unveiled several interesting transition path properties. Thus, we found that the forward and backward transition path times of RTPs on the transition region can

be reduced with increasing particle speed or decreasing tumble rate. We also rigorously prove that the symmetry of the transition path time and shape of the non-equilibrium system of freely diffusing RTPs holds for all system parameters.

This paper provides an example for the study of the transition path dynamics of active matter. Our focus on the transition path dynamics of RTPs reveals the detailed mechanism and non-equilibrium characteristics of the associated dynamics. This work provides the basis for the analysis of other aspects of RTPs and active particle systems, in general. The experimental phenomenon of symmetry breaking of the transition path time observed by Gladrow⁷⁶ in the telegraph process with a potential function motivated this study. Here, we theoretically proved that the transition path time exhibits a symmetry in the absence of a potential function. The symmetry of the transition path time helps us to identify and quantify non-equilibrium dynamics in biological and molecular systems. Berezhkovskii⁷⁰ proved that the transition path time of an equilibrium system is symmetric, regardless of whether the potential function has an asymmetry. The symmetry breaking of the transition path time is a sufficient but not necessary condition for a non-equilibrium system. Therefore, the symmetry of the transition path time may even exist in non-equilibrium systems. This paper provides theoretical examples. We hope that through continuous research on the dynamic behavior of active particles and the realization of more refined methods to control their movement, it will be possible in the future to use active particles for drug delivery and precise guidance, enabling drugs to reach the diseased area accurately.

ACKNOWLEDGMENTS

The authors express their gratitude to the editors and the reviewers for helpful comments. Y. Xu was partially supported by the Key International (Regional) Joint Research Program of the National Science Foundation of China (No. 12120101002). H. Li acknowledges the National Natural Science Foundation of China (No. 12202145). R.M. acknowledges funding from the German Research Foundation (DFG, Grant No. ME 1535/12-1). J. W. Shen acknowledges the National Natural Science Foundation of China (No. 12272135).

AUTHOR DECLARATIONS

Conflict of Interest

The authors have no conflicts to disclose.

Author Contributions

Hua Li: Formal analysis (lead); Writing – original draft (equal). **Yong Xu:** Writing – review & editing (equal). **Ralf Metzler:** Writing – review & editing (equal). **Jianwei Shen:** Writing – review & editing (equal). **Kheder Suleiman:** Writing – review & editing (equal).

DATA AVAILABILITY

Data sharing is not applicable to this article as no new data were created or analyzed in this study.

APPENDIX A: DETAILED THEORETICAL RESULTS FOR THE TRANSIENT PROBABILITY DENSITY FUNCTION

We start by defining the transformation

$$P_{\pm}(x, t|x_0, \sigma_j) = e^{-\gamma t} \bar{P}_{\pm}(x, t|x_0, \sigma_j), \quad (A1)$$

by the help of which Eq. (2) can be rewritten as

$$\frac{\partial P_+(x, t|x_0, \sigma_j)}{\partial t} = -v \frac{\partial}{\partial x} P_+(x, t|x_0, \sigma_j) + \gamma P_-(x, t|x_0, \sigma_j), \quad (A2a)$$

$$\frac{\partial P_-(x, t|x_0, \sigma_j)}{\partial t} = v \frac{\partial}{\partial x} P_-(x, t|x_0, \sigma_j) + \gamma P_+(x, t|x_0, \sigma_j). \quad (A2b)$$

We then apply the Laplace transformation $\bar{f}(s) = \int_0^\infty f(t) \exp(-st) dt$ with respect to t , so that Eqs. (A2) transform into

$$\left[v \frac{\partial}{\partial x} + s \right] \bar{P}_+(x, s|x_0, +1) = \gamma \bar{P}_-(x, s|x_0, +1) + \delta(x - x_0), \quad (A3)$$

$$\left[-v \frac{\partial}{\partial x} + s \right] \bar{P}_-(x, s|x_0, +1) = \gamma \bar{P}_+(x, s|x_0, +1).$$

From these, we find the solutions⁴⁴

$$\begin{aligned} \bar{P}_+(x, s|x_0, +1) &= \frac{s + \alpha \xi}{2v\xi} \left[\{\mathcal{G}(s)\}^{1+\alpha} \mathcal{H}(2x_B - 2x_A - |x_0 - x|, s) \right. \\ &\quad - \{\mathcal{G}(s)\}^{\frac{1+\alpha}{2}} \mathcal{H}(2x_B - x_0 - x, s) \\ &\quad \left. + \mathcal{H}(|x_0 - x|, s) - \{\mathcal{G}(s)\}^{\frac{1+\alpha}{2}} \mathcal{H}(x_0 + x - 2x_A, s) \right] \quad (A4) \end{aligned}$$

and

$$\begin{aligned} \bar{P}_-(x, s|x_0, +1) &= \frac{(s + \xi)(s - \xi)}{2v\xi} \left[\mathcal{H}(|x_0 - x|, s) - \mathcal{H}(2x_B - x_0 - x, s) \right. \\ &\quad \left. - \mathcal{G}(s) \mathcal{H}(x_0 + x - 2x_A, s) + \mathcal{G}(s) \mathcal{H}(2x_B - 2x_A - |x_0 - x|, s) \right], \quad (A5) \end{aligned}$$

where we used the abbreviations

$$\mathcal{G}(s) = \frac{s - \xi(s)}{s + \xi(s)}, \quad (A6a)$$

$$\mathcal{H}(x, s) = \frac{\exp\left(-\frac{\xi x}{v}\right)}{1 - \exp\left(-\frac{(2x_B - 2x_A)\xi}{v}\right)} \mathcal{G}(s), \quad (A6b)$$

and we used $\xi(s) = \sqrt{s^2 - \gamma^2}$.

In the above calculation, we assume that the RTP starts at x_0 and has a positive velocity. We follow a similar approach to obtain the transient probability density $P_{\pm}(x, t|x_0, -1)$ of the particle initially having a “left-moving” state. Due to the symmetry of the transient probability density of the RTP on the transition region

$[x_A, x_B]$, we find

$$P_{\pm}(x, t|x_0, -1) = P_{\mp}(x_B + x_A - x, t|x_B + x_A - x_0, +1). \quad (A7)$$

Hence, we arrive at

$$\begin{aligned} P_+(x, t|x_0, -1) &= P_-(x_B + x_A - x, t|x_B + x_A - x_0, +1) \\ &= \frac{\gamma^2 e^{-\gamma t}}{2v} \left[\mathcal{N}_0(|x_0 - x|, t) - \mathcal{N}_0(x_0 + x - 2x_A, t) \right. \\ &\quad \left. - \mathcal{N}_1(2x_B - x_0 - x, t) + \mathcal{N}_1(2x_B - 2x_A - |x_0 - x|, t) \right] \quad (A8) \end{aligned}$$

and

$$\begin{aligned} P_-(x, t|x_0, -1) &= P_+(x_B + x_A - x, t|x_B + x_A - x_0, +1) \\ &= e^{-\gamma t} \delta(x_0 - x - vt) + \frac{e^{-\gamma t}}{2v} \left[\mathcal{M}_{-\alpha}^0(|x_0 - x|, t) \right. \\ &\quad - \mathcal{M}_{-\alpha}^{\frac{1-\alpha}{2}}(2x_B - x_0 - x, t) - \mathcal{M}_{-\alpha}^{\frac{1-\alpha}{2}}(x_0 + x - 2x_A, t) \\ &\quad \left. + \mathcal{M}_{-\alpha}^{1-\alpha}(2x_B - 2x_A - |x_0 - x|, t) \right]. \quad (A9) \end{aligned}$$

Applying the inverse Laplace transformation leads to Eqs. (8)–(13).

APPENDIX B: DETAILED THEORETICAL RESULTS FOR THE MEAN TRANSITION PATH TIME AND TRANSITION PATH SHAPE

From Eq. (17), we deduce

$$\begin{aligned} v \frac{\partial}{\partial x_0} K^{(1)}(x_A|x_0, +1) + \gamma [K^{(1)}(x_A|x_0, -1) - K^{(1)}(x_A|x_0, +1)] &= -\phi_A(x_0, +1), \quad (B1) \\ v \frac{\partial}{\partial x_0} K^{(1)}(x_A|x_0, -1) + \gamma [K^{(1)}(x_A|x_0, +1) - K^{(1)}(x_A|x_0, -1)] &= -\phi_A(x_0, -1). \end{aligned}$$

We define $\chi(x_0) = K^{(1)}(x_A|x_0, +1) + K^{(1)}(x_A|x_0, -1)$ and $\zeta(x_0) = K^{(1)}(x_A|x_0, +1) - K^{(1)}(x_A|x_0, -1)$. Then, Eq. (B1) can be rewritten as

$$\begin{aligned} v \frac{\partial}{\partial x_0} \zeta(x_0) &= -2\phi_A(x_0), \quad (B2) \\ v \frac{\partial}{\partial x_0} \chi(x_0) - 2\gamma \zeta(x_0) &= \phi_A(x_0, -1) - \phi_A(x_0, +1). \end{aligned}$$

Then,

$$\zeta(x_0) = \frac{2}{v} \int_{x_0}^{x_B} \phi_A(y) dy + N_1, \tag{B3}$$

$$\begin{aligned} \chi(x_0) = & -\frac{4\gamma}{v^2} \int_{x_0}^{x_B} \int_y^{x_B} \phi_A(z) dz dy - \frac{2\gamma}{v} N_1 (x_B - x_0) \\ & - \frac{1}{v} \int_{x_0}^{x_B} \phi_A(y, -1) dy + \frac{1}{v} \int_{x_0}^{x_B} \phi_A(y, +1) dy + N_2, \end{aligned}$$

where

$$\begin{aligned} N_1 = & -\frac{v}{\gamma(x_B - x_A) + v} \left[\frac{2\gamma}{v^2} \int_{x_A}^{x_B} \int_y^{x_B} \phi_A(z) dz dy \right. \\ & + \frac{1}{2v} \int_{x_A}^{x_B} \phi_A(y, -1) dy - \frac{1}{2v} \int_{x_A}^{x_B} \phi_A(y, +1) dy \\ & \left. + \frac{1}{v} \int_{x_A}^{x_B} \phi_A(y) dy \right], \tag{B4} \end{aligned}$$

$$N_2 = -N_1.$$

Then, $K^{(1)}(x_A|x_0, \pm 1) = \frac{1}{2}[\zeta(x_0) + \chi(x_0)]$.

Equations (28) and (B4) can be further simplified according to the following results:

$$\begin{aligned} Z_1 = & \int_{x_A}^{x_B} \int_y^{x_B} \phi_B(z) dz dy \\ = & \frac{n_1}{2} \left((\gamma x_B^2 + n_2 x_B)(x_B - x_A) - \frac{\gamma}{3}(x_B^3 - x_A^3) - \frac{n_2}{2}(x_B^2 - x_A^2) \right), \\ Z_2 = & \int_{x_A}^{x_B} \phi_B(y, -1) dy - \int_{x_A}^{x_B} \phi_B(y, +1) dy = -\frac{1}{2} n_1 (x_B - x_A), \\ Z_3 = & \int_{x_A}^{x_B} \phi_B(y) dy = \frac{1}{2} (x_B - x_A), \tag{B5} \\ C_1 = & -vn_1 \left(\frac{2\gamma}{v^2} Z_1 + Z_2 + \frac{1}{v} Z_3 \right), \\ C_2 = & C_1 + \frac{2}{v} Z_3, \end{aligned}$$

and

$$\begin{aligned} Y_1 = & \int_{x_A}^{x_B} \int_y^{x_B} \phi_A(z) dz dy \\ = & \frac{n_1}{2} \left((n_3 x_B - \gamma x_B^2)(x_B - x_A) + \frac{\gamma}{3}(x_B^3 - x_A^3) - \frac{n_3}{2}(x_B^2 - x_A^2) \right), \\ Y_2 = & \int_{x_A}^{x_B} \phi_A(y, -1) dy - \int_{x_A}^{x_B} \phi_A(y, +1) dy = \frac{1}{2} n_1 (x_B - x_A), \\ Y_3 = & \int_{x_A}^{x_B} \phi_A(y) dy = Z_3, \tag{B6} \\ N_1 = & -vn_1 \left(\frac{2\gamma}{v^2} Y_1 + Y_2 + \frac{1}{v} Y_3 \right), \\ N_2 = & -N_1, \end{aligned}$$

where $n_1 = \frac{1}{v+\gamma(x_B-x_A)}$, $n_2 = v - 2\gamma x_A$, $n_3 = v + 2\gamma x_B$.

In order to prove that $C_2 = N_2$, we continue to simplify these expressions, obtaining

$$\begin{aligned} Y_1 = & \frac{1}{2}(x_B - x_A)^2 - Z_1, \\ C_2 = & -vn_1 \left(\frac{2\gamma}{v^2} Z_1 + Z_2 \right) + (2 - n_1 v) \frac{1}{v} Z_3, \tag{B7} \\ N_2 = & -vn_1 \left(\frac{2\gamma}{v^2} Z_1 + Z_2 \right) + \frac{\gamma n_1}{v} (x_B - x_A)^2 + n_1 Z_3 = C_2. \end{aligned}$$

Therefore, forward and reverse transition path times, $\tau^{TP}(x_B|x_A)$ and $\tau^{TP}(x_A|x_B)$, are indeed equal.

For the transition path shape, Eq. (33) can be written as

$$\begin{aligned} \tau_{\text{shape}}^{TP}(x_0|x_A) = & \frac{K^{(1)}(x_A|x_0)}{\phi_A(x_0)}, \tag{B8} \\ \tau_{\text{shape}}^{TP}(x_0|x_B) = & \frac{K^{(1)}(x_B|x_0)}{\phi_B(x_0)}. \end{aligned}$$

Then, Eqs. (27) and (B3) can be further simplified to yield

$$\begin{aligned} S_1(x_0) = & \int_{x_A}^{x_0} \int_y^{x_B} \phi_B(z) dz dy, \\ = & \frac{1}{2} \left[(\gamma x_B^2 + n_2 x_B)(x_0 - x_A) - \frac{1}{3}(x_0^3 - x_A^3) - \frac{1}{2} n_2 (x_0^2 - x_A^2) \right], \\ S_2(x_0) = & \frac{1}{v} \int_{x_A}^{x_0} \phi_B(y, -1) dy - \frac{1}{v} \int_{x_A}^{x_0} \phi_B(y, +1) dy = -n_1 (x_0 - x_A), \\ S_3(x_0) = & \int_{x_0}^{x_B} \int_y^{x_B} \phi_A(z) dz dy, \\ = & \frac{1}{2} \left[(n_3 x_B - \gamma x_B^2)(x_B - x_0) - \frac{1}{3}(x_B^3 - x_0^3) - \frac{1}{2} n_3 (x_B^2 - x_0^2) \right], \tag{B9} \end{aligned}$$

$$S_4(x_0) = -\frac{1}{v} \int_{x_0}^{x_B} \phi_A(y, -1) dy + \frac{1}{v} \int_{x_0}^{x_B} \phi_A(y, +1) dy = -n_1 (x_B - x_0),$$

$$\eta(x_0) = \frac{4\gamma}{v^2} S_1(x_0) + \frac{2\gamma}{v} C_1 (x_0 - x_A) + S_2(x_0) + C_2,$$

$$\chi(x_0) = -\frac{4\gamma}{v^2} S_3(x_0) - \frac{2\gamma}{v} N_1 (x_B - x_0) + S_4(x_0) + N_2.$$

For $x_0 \in [x_A, x_B]$, the symmetry point of x_0 over the interval $[x_A, x_B]$ is $x_B + x_A - x_0$, according to Eqs. (24) and (B9), so that we obtain

$$\begin{aligned} K^{(1)}(x_B|x_B + x_A - x_0) = & K^{(1)}(x_A|x_0), \\ \phi_B(x_B + x_A - x_0) = & \phi_A(x_0), \tag{B10} \\ \tau_{\text{shape}}^{TP}(x_B + x_A - x_0|x_B) = & \tau_{\text{shape}}^{TP}(x_0|x_A), \end{aligned}$$

i.e., $\tau_{\text{shape}}^{TP}(x_0|x_B)$ and $\tau_{\text{shape}}^{TP}(x_0|x_A)$ are symmetric over the interval $[x_A, x_B]$.

APPENDIX C: DETAILED THEORETICAL RESULTS FOR THE COEFFICIENT OF VARIATION

We here provide theoretical results for the coefficient of variation of the transition path time distribution. To this end, we calculate the second moments of the first passage time distributions. According to Eq. (17),

$$-2K^{(1)}(x_{A/B}|x_0, +1) = v \frac{\partial}{\partial x_0} K^{(2)}(x_{A/B}|x_0, +1) + \gamma [K^{(2)}(x_{A/B}|x_0, -1) - K^{(2)}(x_{A/B}|x_0, +1)], \tag{C1}$$

$$-2K^{(1)}(x_{A/B}|x_0, -1) = -v \frac{\partial}{\partial x_0} K^{(2)}(x_{A/B}|x_0, +1) + \gamma [K^{(2)}(x_{A/B}|x_0, +1) - K^{(2)}(x_{A/B}|x_0, -1)].$$

Similarly, we define $\lambda(x_0) = K^{(2)}(x_B|x_0, +1) + K^{(2)}(x_B|x_0, -1)$ and $\tau(x_0) = K^{(2)}(x_B|x_0, +1) - K^{(2)}(x_B|x_0, -1)$. Then, Eq. (C1) turns into

$$v \frac{\partial}{\partial x_0} \tau(x_0) = -4K^{(1)}(x_B|x_0), \tag{C2}$$

$$v \frac{\partial}{\partial x_0} \lambda(x_0) = 2\gamma \tau(x_0) + 2 [K^{(1)}(x_B|x_0, -1) - K^{(1)}(x_B|x_0, +1)].$$

Invoking the boundary conditions, we obtain

$$\tau(x_0) = \frac{4}{v} \int_{x_0}^{x_B} K^{(1)}(x_B|y) dy + M_1, \tag{C3}$$

$$\lambda(x_0) = \frac{8\gamma}{v^2} \int_{x_A}^{x_0} \int_y^{x_B} K^{(1)}(x_B|z) dz dy + \frac{2\gamma}{v} N_1(x_0 - x_A) M_1 + \frac{2}{v} \int_{x_A}^{x_0} K^{(1)}(x_B|y, -1) dy - \frac{2}{v} \int_{x_A}^{x_0} K^{(1)}(x_B|y, +1) dy + M_2,$$

where we introduced

$$M_1 = -\frac{v}{\gamma(x_B - x_A) + v} \left[\frac{4\gamma}{v^2} \int_{x_A}^{x_B} \int_y^{x_B} K^{(1)}(x_B|z) dz dy + \frac{1}{v} \int_{x_A}^{x_B} K^{(1)}(x_B|y, -1) dy - \frac{1}{v} \int_{x_A}^{x_B} K^{(1)}(x_B|y, +1) dy + \frac{2}{v} \int_{x_A}^{x_B} K^{(1)}(x_B|y) dy \right], \tag{C4}$$

$$M_2 = M_1 + \frac{4}{v} \int_{x_A}^{x_B} K^{(1)}(x_B|y) dy.$$

Then, $K^{(2)}(x_B|x_A) = \frac{M_2}{2}$, and the second moment of the forward transition path time is

$$\langle t_{TP}^2 \rangle = \frac{K^{(2)}(x_B|x_A)}{\phi_B(x_A)}. \tag{C5}$$

Similarly, we define $\omega(x_0) = K^{(2)}(x_A|x_0, +1) + K^{(2)}(x_A|x_0, -1)$ and $\beta(x_0) = K^{(2)}(x_A|x_0, +1) - K^{(2)}(x_A|x_0, -1)$. We then find

$$\beta(x_0) = \frac{4}{v} \int_{x_0}^{x_B} K^{(1)}(x_A|y) dy + M_3, \tag{C6}$$

$$\omega(x_0) = \frac{8\gamma}{v^2} \int_{x_A}^{x_0} \int_y^{x_B} K^{(1)}(x_A|z) dz dy + \frac{2\gamma}{v} M_3(x_0 - x_A) + \frac{2}{v} \int_{x_A}^{x_0} K^{(1)}(x_A|y, -1) dy - \frac{2}{v} \int_{x_A}^{x_0} K^{(1)}(x_A|y, +1) dy + M_4,$$

where

$$M_3 = -\frac{v}{\gamma(x_B - x_A) + v} \left[\frac{4\gamma}{v^2} \int_{x_A}^{x_B} \int_y^{x_B} K^{(1)}(x_A|z) dz dy - \frac{1}{v} \int_{x_A}^{x_0} K^{(1)}(x_A|y, -1) dy + \frac{1}{v} \int_{x_A}^{x_0} K^{(1)}(x_A|y, +1) dy - \frac{2}{v} \int_{x_A}^{x_B} K^{(1)}(x_A|y) dy \right], \tag{C7}$$

$$M_4 = M_3 + \frac{4}{v} \int_{x_A}^{x_B} K^{(1)}(x_A|y) dy.$$

Therefore, the second moment of the reverse transition path time is

$$\langle t_{TP}^2 \rangle = \frac{K^{(2)}(x_A|x_B)}{\phi_A(x_B)}, \tag{C8}$$

where $K^{(2)}(x_A|x_B) = \frac{M_4}{2}$. Hence, the coefficient of variation of the transition path time distribution in the two directions can be derived from Eqs. (C5) and (C8).

REFERENCES

- ¹M. C. Marchetti, J. F. Joanny, S. Ramaswamy, T. B. Liverpool, J. Prost, M. Rao, and R. A. Simha, "Hydrodynamics of soft active matter," *Rev. Mod. Phys.* **85**, 1143 (2013).
- ²C. Bechinger, R. Di Leonardo, H. Löwen, C. Reichhardt, G. Volpe, and G. Volpe, "Active particles in complex and crowded environments," *Rev. Mod. Phys.* **88**, 045006 (2016).
- ³S. Ramaswamy, "Active matter," *J. Stat. Mech.: Theory Exp.* **2017**, 054002.
- ⁴A. Pikovsky, "Deterministic active particles in the overactive limit," *Chaos* **33**, 113114 (2023).
- ⁵K. Goswami, A. G. Cherstvy, A. Godec, and R. Metzler, "Anomalous diffusion of active Brownian particles in responsive elastic gels: Nonergodicity, non-Gaussianity, and distributions of trapping times," *Phys. Rev. E* **110**, 044609 (2024).
- ⁶R. N. Valani, "Infinite-memory classical wave-particle entities, attractor-driven active particles, and the diffusionless Lorenz equations," *Chaos* **34**, 013133 (2024).
- ⁷C. Spaulding, H. Teimouri, S. L. Narasimhan, and A. B. Kolomeisky, "The role of extended range of interactions in the dynamics of interacting molecular motors," *J. Phys. A-Math. Theor.* **55**, 255601 (2022).
- ⁸B. Stuhmann, M. Soares e Silva, M. Depken, F. C. MacKintosh, and G. H. Koenderink, "Nonequilibrium fluctuations of a remodeling *in vitro* cytoskeleton," *Phys. Rev. E* **86**, 020901 (2012).
- ⁹A. B. Kolomeisky, *Motor Proteins and Molecular Motors* (CRC Press, New York, 2015).
- ¹⁰D. Feldmann, P. Arya, N. Lomadze, A. Kopyshv, and S. Santer, "Light-driven motion of self-propelled porous Janus particles," *Appl. Phys. Lett.* **115**, 263701 (2019).

- ¹¹C. Wilhelm, “Out-of-equilibrium microrheology inside living cells,” *Phys. Rev. Lett.* **101**, 028101 (2008).
- ¹²H. Teimouri, A. Medvedeva, and A. B. Kolomeisky, “Bacteria-specific feature selection for enhanced antimicrobial peptide activity predictions using machine-learning methods,” *J. Chem. Inf. Model.* **63**, 1723 (2023).
- ¹³N. Kumar, H. Soni, S. Ramaswamy, and A. K. Sood, “Flocking at a distance in active granular matter,” *Nat. Commun.* **5**, 4688 (2014).
- ¹⁴J. Jhavar, R. G. Morris, U. R. Amith-Kumar, M. Danny Raj, T. Rogers, H. Rajendran, and V. Guttal, “Noise-induced schooling of fish,” *Nat. Phys.* **16**, 488 (2020).
- ¹⁵R. Ross, “The logical basis of the sanitary policy of mosquito reduction,” *Science* **22**, 689 (1905).
- ¹⁶K. Pearson, “The problem of the random walk,” *Nature* **72**, 294 (1905).
- ¹⁷See https://embryology.med.unsw.edu.au/embryology/index.php/Movie_-_Neutrophil_chasing_bacteria for a short explanation and a link to the movie.
- ¹⁸H. C. Berg and R. A. Anderson, “Bacteria swim by rotating their flagellar filaments,” *Nature* **245**, 380 (1973).
- ¹⁹C. W. Reynolds, “Flocks, herds and schools: A distributed behavioral model,” *Comput. Graph.* **21**, 25–34 (1987).
- ²⁰T. Vicsek, A. Czirók, E. Ben-Jacob, I. Cohen, and O. Shochet, “Novel type of phase transition in a system of self-driven particles,” *Phys. Rev. Lett.* **75**, 1226 (1995).
- ²¹S. J. Ebbens and J. R. Howse, “In pursuit of propulsion at the nanoscale,” *Soft Matter* **6**, 726 (2010).
- ²²E. Lemaître, I. M. Sokolov, R. Metzler, and V. Aleksei Chechkin, “Non-Gaussian displacement distributions in models of heterogeneous active particle dynamics,” *New J. Phys.* **25**, 013010 (2023).
- ²³C. Kurzthaler, Y. Zhao, N. Zhou, J. Schwarz-Linek, C. Devailly, J. Arlt, J. Huang, W. C. K. Poon, T. Franosch, J. Tailleur, and V. A. Martinez, “Characterization and control of the run-and-tumble dynamics of *Escherichia coli*,” *Phys. Rev. Lett.* **132**, 038302 (2024).
- ²⁴B. Loewe, T. Kozhukhov, and T. N. Shendruk, “Anisotropic run-and-tumble-turn dynamics,” *Soft Matter* **20**, 1133 (2024).
- ²⁵H. C. Berg, *E. coli in Motion* (Springer, New York, 2004).
- ²⁶N. R. Smith, P. Le Doussal, S. N. Majumdar, and G. Schehr, “Exact position distribution of a harmonically confined run-and-tumble particle in two dimensions,” *Phys. Rev. E* **106**, 054133 (2022).
- ²⁷T. Chakraborty and P. Pradhan, “Time-dependent properties of run-and-tumble particles: Density relaxation,” *Phys. Rev. E* **109**, 024124 (2024).
- ²⁸G. Tucci, A. Gambassi, S. N. Majumdar, and G. Schehr, “First-passage time of run-and-tumble particles with noninstantaneous resetting,” *Phys. Rev. E* **106**, 044127 (2022).
- ²⁹K. S. Olsen, “Steady-state moments under resetting to a distribution,” *Phys. Rev. E* **108**, 044120 (2023).
- ³⁰T. Banerjee, S. N. Majumdar, A. Rosso, and G. Schehr, “Current fluctuations in noninteracting run-and-tumble particles in one dimension,” *Phys. Rev. E* **101**, 052101 (2020).
- ³¹P. Le Doussal, S. N. Majumdar, and G. Schehr, “Velocity and diffusion constant of an active particle in a one-dimensional force field,” *EPL-Europhys. Lett.* **130**, 40002 (2020).
- ³²C. Roberts and Z. Zhen, “Run-and-tumble motion in a linear ratchet potential: Analytic solution, power extraction, and first-passage properties,” *Phys. Rev. E* **108**, 014139 (2023).
- ³³E. Jeon, B. G. Go, and Y. W. Kim, “Searching for a partially absorbing target by a run-and-tumble particle in a confined space,” *Phys. Rev. E* **109**, 014103 (2024).
- ³⁴R. Garcia-Millan and G. Pruessner, “Run-and-tumble motion in a harmonic potential: Field theory and entropy production,” *J. Stat. Mech.* **2021**, 063203.
- ³⁵P. Padmanabha, D. M. Busiello, A. Maritan, and D. Gupta, “Fluctuations of entropy production of a run-and-tumble particle,” *Phys. Rev. E* **107**, 014129 (2023).
- ³⁶A. Dhar, A. Kundu, S. N. Majumdar, S. Sabhapandit, and G. Schehr, “Run-and-tumble particle in one-dimensional confining potentials: Steady-state, relaxation, and first-passage properties,” *Phys. Rev. E* **99**, 032132 (2019).
- ³⁷F. J. Sevilla, A. V. Arzola, and E. P. Cital, “Stationary superstatistics distributions of trapped run-and-tumble particles,” *Phys. Rev. E* **99**, 012145 (2019).
- ³⁸C. G. Wagner, M. F. Hagan, and A. Baskaran, “Steady-state distributions of ideal active Brownian particles under confinement and forcing,” *J. Stat. Mech.: Theory Exp.* **2017**, 043203.
- ³⁹H. H. Wensink and H. Löwen, “Aggregation of self-propelled colloidal rods near confining walls,” *Phys. Rev. E* **78**, 031409 (2008).
- ⁴⁰L. Angelani, “Confined run-and-tumble swimmers in one dimension,” *J. Phys. A-Math. Theor.* **50**, 325601 (2017).
- ⁴¹M. R. Evans and S. N. Majumdar, “Run and tumble particle under resetting: A renewal approach,” *J. Phys. A-Math. Theor.* **51**, 475003 (2018).
- ⁴²O. Dauchot and V. Démery, “Dynamics of a self-propelled particle in a harmonic trap,” *Phys. Rev. Lett.* **122**, 068002 (2019).
- ⁴³P. Singh and A. Kundu, “Generalised ‘Arcsine’ laws for run-and-tumble particle in one dimension,” *J. Stat. Mech.* **2019**, 083205.
- ⁴⁴P. Singh, S. Santra, and A. Kundu, “Extremal statistics of a one-dimensional run and tumble particle with an absorbing wall,” *J. Phys. A-Math. Theor.* **55**, 465004 (2022).
- ⁴⁵H. S. Chung, K. McHale, J. M. Louis, and W. A. Eaton, “Single-molecule fluorescence experiments determine protein folding transition path times,” *Science* **335**, 981 (2012).
- ⁴⁶G. Hummer, “From transition paths to transition states and rate coefficients,” *J. Chem. Phys.* **120**, 516 (2004).
- ⁴⁷A. Godec and D. E. Makarov, “Challenges in inferring the directionality of active molecular processes from single-molecule fluorescence resonance energy transfer trajectories,” *J. Phys. Chem. Lett.* **14**, 49 (2022).
- ⁴⁸B. Zhang, D. Jasnow, and D. M. Zuckerman, “Transition-event durations in one-dimensional activated processes,” *J. Chem. Phys.* **126**, 74504 (2007).
- ⁴⁹R. Satija, A. M. Berezhkovskii, and D. E. Makarov, “Broad distributions of transition-path times are fingerprints of multidimensionality of the underlying free energy landscapes,” *Proc. Natl. Acad. Sci. U.S.A.* **117**, 27116 (2020).
- ⁵⁰Y. Xu, H. Li, H. Wang, W. Jia, X. Yue, and J. Kurths, “The estimates of the mean first exit time of a bistable system excited by Poisson white noise,” *J. Appl. Mech.* **84**, 091004 (2017).
- ⁵¹D. K. Lubensky and D. R. Nelson, “Driven polymer translocation through a narrow pore,” *Biophys. J.* **77**, 1824 (1999).
- ⁵²D. Hartich and A. Godec, “Emergent memory and kinetic hysteresis in strongly driven networks,” *Phys. Rev. X* **11**, 041047 (2021).
- ⁵³A. M. Berezhkovskii and D. E. Makarov, “On distributions of barrier crossing times as observed in single-molecule studies of biomolecules,” *Biophys. Rep.* **1**, 100029 (2021).
- ⁵⁴W. K. Kim and R. R. Netz, “The mean shape of transition and first-passage paths,” *J. Chem. Phys.* **143**, 224108 (2015).
- ⁵⁵G. M. Torrie and J. P. Valleau, “Nonphysical sampling distributions in Monte Carlo free-energy estimation: Umbrella sampling,” *J. Comput. Phys.* **23**, 187 (1977).
- ⁵⁶T. S. Van Erp and P. G. Bolhuis, “Elaborating transition interface sampling methods,” *J. Comput. Phys.* **205**, 157 (2005).
- ⁵⁷W. N. E., W. Ren, and E. Vanden-Eijnden, “String method for the study of rare events,” *Phys. Rev. B* **66**, 052301 (2002).
- ⁵⁸K. Blom, K. Song, E. Vouga, and D. E. Makarov, “Milestoning estimators of dissipation in systems observed at a coarse resolution,” *Proc. Natl. Acad. Sci. U.S.A.* **121**, e2318333121 (2024).
- ⁵⁹A. K. Faradjian and R. Elber, “Computing time scales from reaction coordinates by milestoning,” *J. Chem. Phys.* **120**, 10880 (2004).
- ⁶⁰R. J. Allen, D. Frenkel, and P. R. Ten Wolde, “Forward flux sampling-type schemes for simulating rare events: Efficiency analysis,” *J. Chem. Phys.* **124**, 194111 (2006).
- ⁶¹M. M. Reiner, B. Bachmair, M. X. Tiefenbacher, S. Mai, L. González, P. Marquetand, and C. Dellago, “Nonadiabatic forward flux sampling for excited-state rare events,” *J. Chem. Theory Comput.* **19**, 1657 (2023).
- ⁶²X. L. Wang, J. Feng, Y. Xu, and J. Kurths, “Deep learning-based state prediction of the Lorenz system with control parameters,” *Chaos* **34**, 033108 (2024).
- ⁶³L. Bonati, G. M. Piccini, and M. Parrinello, “Deep learning the slow modes for rare events sampling,” *Proc. Natl. Acad. Sci. U.S.A.* **118**, e2113533118 (2021).
- ⁶⁴H. Zhang, Y. Xu, Q. Liu, and Y. G. Li, “Deep learning framework for solving Fokker-Planck equations with low-rank separation representation,” *Eng. Appl. Artif. Intel.* **121**, 106036 (2023).

- ⁶⁵E. Medina, R. Satija, and D. E. Makarov, "Transition path times in non-Markovian activated rate processes," *J. Phys. Chem. B* **122**, 11400 (2018).
- ⁶⁶H. Li, Y. Xu, R. Metzler, and J. W. Shen, "Transition path properties for one-dimensional non-Markovian models," *J. Phys. A-Math. Theor.* **57**, 355201 (2024).
- ⁶⁷D. E. Makarov, "Reconciling transition path time and rate measurements in reactions with large entropic barriers," *J. Chem. Phys.* **146**, 071101 (2017).
- ⁶⁸A. M. Berezhkovskii and D. E. Makarov, "Communication: Transition-path velocity as an experimental measure of barrier crossing dynamics," *J. Chem. Phys.* **148**, 201102 (2018).
- ⁶⁹H. Li, Y. Xu, Y. G. Li, and R. Metzler, "Transition path dynamics across rough inverted parabolic potential barrier," *Eur. Phys. J. Plus* **135**, 731 (2020).
- ⁷⁰A. M. Berezhkovskii, G. Hummer, and S. M. Bezrukov, "Identity of distributions of direct uphill and downhill translocation times for particles traversing membrane channels," *Phys. Rev. Lett.* **97**, 020601 (2006).
- ⁷¹D. Singh, K. Mondal, and S. Chaudhury, "Effect of memory and inertial contribution on transition-time distributions: Theory and simulations," *J. Phys. Chem. B* **125**, 4536 (2021).
- ⁷²A. M. Berezhkovskii and D. E. Makarov, "On the forward/backward symmetry of transition path time distributions in nonequilibrium systems," *J. Chem. Phys.* **151**, 065102 (2019).
- ⁷³R. Satija, A. Das, and D. E. Makarov, "Transition path times reveal memory effects and anomalous diffusion in the dynamics of protein folding," *J. Chem. Phys.* **147**, 152707 (2017).
- ⁷⁴D. Janakiraman, "Transition path time distributions for Lévy flights," *J. Phys. A-Math. Theor.* **51**, 285001 (2018).
- ⁷⁵H. Li, Y. Xu, R. Metzler, and J. Kurths, "Transition path properties for one-dimensional systems driven by Poisson white noise," *Chaos, Soliton. Fract.* **141**, 110293 (2020).
- ⁷⁶J. Gladrow, M. Ribezzi-Crivellari, F. Ritort, and U. F. Keyser, "Experimental evidence of symmetry breaking of transition-path times," *Nat. Commun.* **10**, 55 (2019).
- ⁷⁷J. J. Kasianowicz, E. Brandin, D. Branton, and D. W. Deamer, "Characterization of individual polynucleotide molecules using a membrane channel," *Proc. Natl. Acad. Sci. U.S.A.* **93**, 13770 (1996).
- ⁷⁸K. R. Mahendran, C. Chimerel, T. Mach, and M. Winterhalter, "Antibiotic translocation through membrane channels: Temperature-dependent ion current fluctuation for catching the fast events," *Eur. Biophys. J. Biophys.* **38**, 1141 (2009).
- ⁷⁹J. Um, T. Song, and J. H. Jeon, "Langevin dynamics driven by a telegraphic active noise," *Front. Phys.* **7**, 143 (2019).
- ⁸⁰R. N. Valani and D. M. Paganin, "Attractor-driven matter," *Chaos* **33**, 023125 (2023).
- ⁸¹K. Kawaguchi, R. Kageyama, and M. Sano, "Topological defects control collective dynamics in neural progenitor cell cultures," *Nature* **545**, 327 (2017).
- ⁸²C. K. Schmidt, M. Medina-Sánchez, R. J. Edmondson, and O. G. Schmidt, "Engineering microrobots for targeted cancer therapies from a medical perspective," *Nat. Commun.* **11**, 5618 (2020).
- ⁸³F. Di Trapani, T. Franosch, and M. Caraglio, "Active Brownian particles in a circular disk with an absorbing boundary," *Phys. Rev. E* **107**, 064123 (2023).
- ⁸⁴J. Tailleur and M. E. Cates, "Statistical mechanics of interacting run-and-tumble bacteria," *Phys. Rev. Lett.* **100**, 218103 (2008).
- ⁸⁵L. Cocconi, J. Knight, and C. Roberts, "Optimal power extraction from active particles with hidden states," *Phys. Rev. Lett.* **131**, 188301 (2023).
- ⁸⁶D. Barik, P. K. Ghosh, and D. S. Ray, "Langevin dynamics with dichotomous noise: Direct simulation and applications," *J. Stat. Mech.* **2006**, P03010.